Chinese Journal of Chemical Engineering 74 (2024) 295–311

Contents lists available at ScienceDirect

Chinese Journal of Chemical Engineering

journal homepage: www.elsevier.com/locate/CJChE

Full Length Article

Stochastic neuro-swarming intelligence paradigm for the analysis of magneto-hydrodynamic Prandtl–Eyring fluid flow with diffusive magnetic layers effect over an elongated surface

Zeeshan Ikram Butt [1], Iftikhar Ahmad [1], Muhammad Shoaib [2], Syed Ibrar Hussain [3,4,*], Hira Ilyas [5], Muhammad Asif Zahoor Raja [6]

[1] Department of Mathematics, University of Gujrat, Gujrat 50700, Pakistan
[2] Yuan Ze University, AI Center, Taoyuan, Taiwan 320, China
[3] Department of Mathematics and Computer Science, University of Palermo, Via Archirafi 34, Palermo 90123, Italy
[4] Department of Mathematics, University of Houston, Houston, TX 77204, USA
[5] Department of Physical Sciences, University of Chenab, Gujrat 50700, Pakistan
[6] Future Technology Research Centre, National Yunlin University of Science and Technology, Yunlin, Taiwan 64002, China

ARTICLE INFO

Article history:
Received 6 March 2024
Received in revised form
5 July 2024
Accepted 8 July 2024
Available online 23 July 2024

Keywords:
Prandtl–Eyring fluid
Particle swarm optimization
Hydrodynamic
Neural networks
Computational fluid dynamics

ABSTRACT

In recent years, the integration of stochastic techniques, especially those based on artificial neural networks, has emerged as a pivotal advancement in the field of computational fluid dynamics. These techniques offer a powerful framework for the analysis of complex fluid flow phenomena and address the uncertainties inherent in fluid dynamics systems. Following this trend, the current investigation portrays the design and construction of an important technique named swarming optimized neuro-heuristic intelligence with the competency of artificial neural networks to analyze nonlinear visco-elastic magneto-hydrodynamic Prandtl–Eyring fluid flow model, with diffusive magnetic layers effect along an extended sheet. The currently designed computational technique is established using inverse multiquadric radial basis activation function through the hybridization of a well-known global searching technique of particle swarm optimization and sequential quadratic programming, a technique capable of rapid convergence locally. The most appropriate scaling group involved transformations that are implemented on governing equations of the suggested fluidic model to convert it from a system of nonlinear partial differential equations into a dimensionless form of a third-order nonlinear ordinary differential equation. The transformed/reduced fluid flow model is solved for sundry variations of physical quantities using the designed scheme and outcomes are matched consistently with Adam's numerical technique with negligible magnitude of absolute errors and mean square errors. Moreover, it is revealed that the velocity of the fluid depreciates in the presence of a strong magnetic field effect. The efficacy of the designed solver is depicted evidently through rigorous statistical observations *via* exhaustive numerical experimentation of the fluidic problem.

1. Introduction

Magnetohydrodynamic (MHD) is a subclass of fluid dynamics in which electrically conducting fluid characteristics are analyzed. Fluids including salt water, electrolysis, and plasma are some common examples of MHD. Some common applications of MHD are electromagnetic propulsion, pumps, and power generators successfully playing their role in industries. MHD's extensive use attracts many researchers to examine various fluids in the presence of the magnetic field. Mishra *et al.* [1] investigated MHD radiative flow over an exponentially stretching surface (ST-S) under the effect of the magnetic field. Abdul Jawwad *et al.* [2] examined MHD Carreau nanofluid over radially ST-S in the case of stagnation point flow. Mahabaleshwar *et al.* [3] scrutinized flow in MHD Casson fluid with chemical reaction impact. Alqahtani *et al.* [4] discussed the heat transfer effect *via* MHD Darcy–Forchheimer Casson fluid along an exponential ST-S. Al-Bossly *et al.* [5] studied MHD phenomena in

* Corresponding author.
E-mail addresses: syedibrar.hussain@unipa.it, syedhussain.ibrar@gmail.com (S.I. Hussain).

https://doi.org/10.1016/j.cjche.2024.07.001

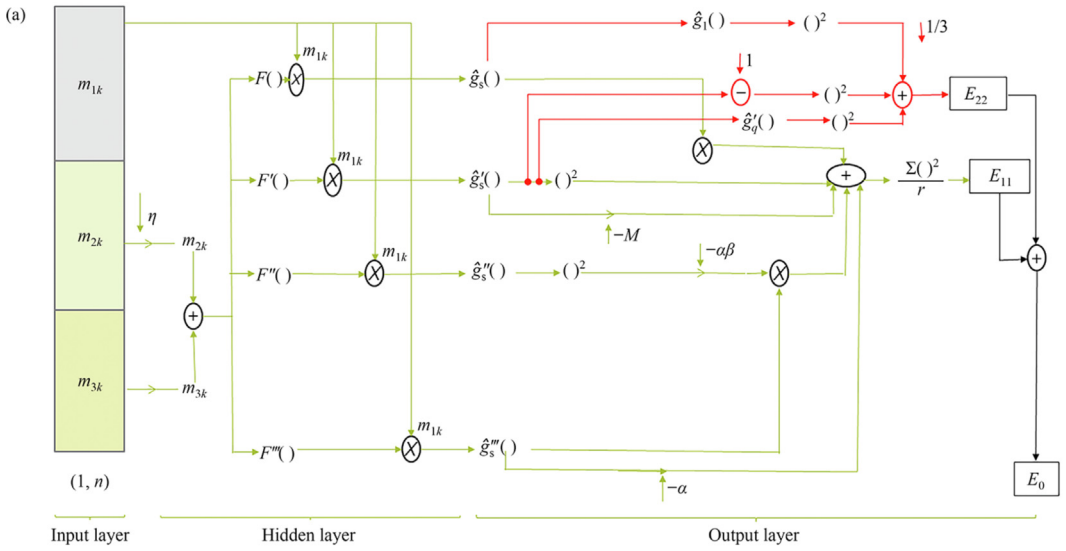

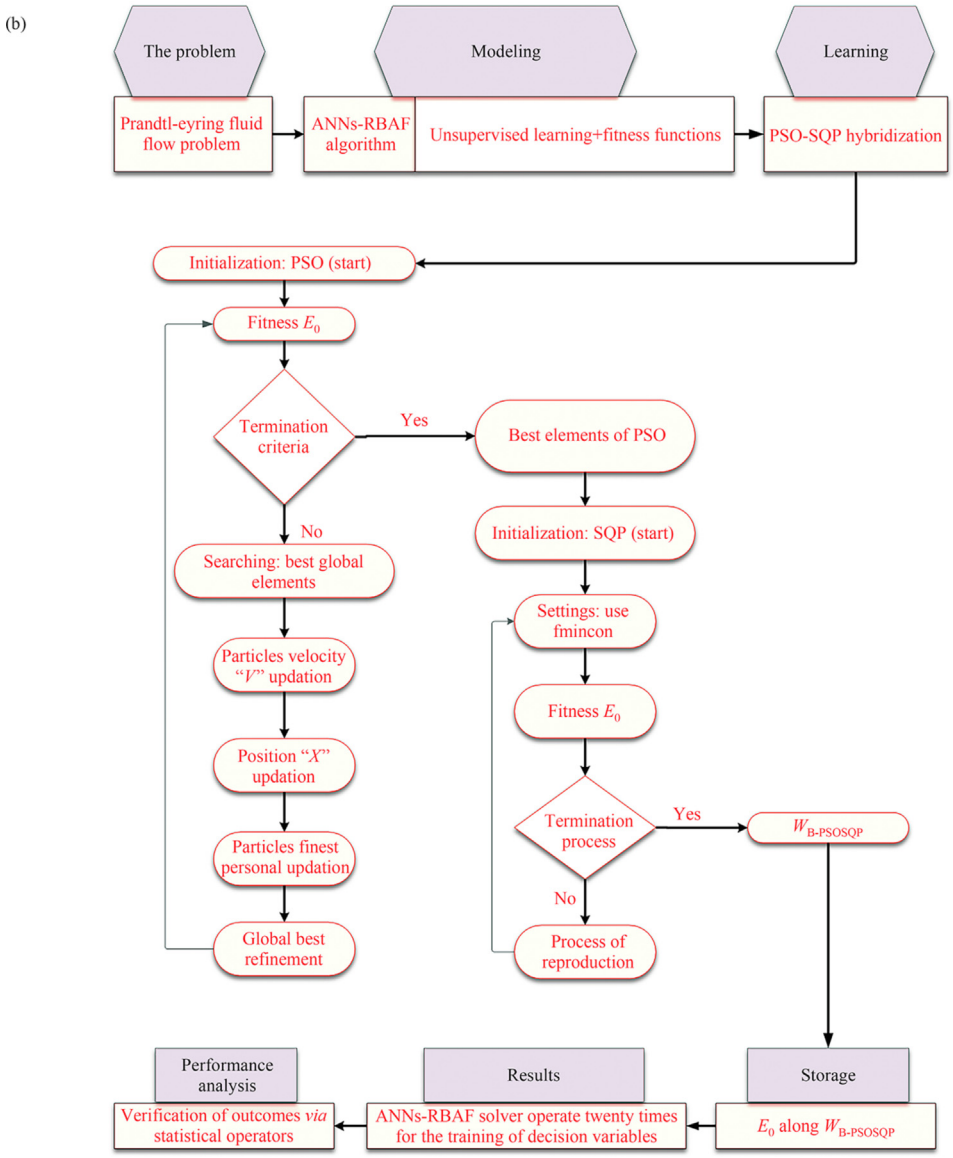

Fig. 1. (a) Structure diagram of ANNs-RBAF-PSO algorithm to solve MHD-PEFF problem. (b) Graphical abstract designed for ANNs-RBAF-PSO algorithm to solve MHD-PEFF problem.

Eyring–Powell fluid with mixed convection along ST-S. Bhatti and Michaelides [6] formulated Oldroyd 6-constant fluid using microplates under the influence of electro-MHD. Shahid *et al.* [7] numerically investigated a fluid containing nanoparticles through a porous medium with the MHD effect. MHD-based productive research is presented in Refs. [8–15].

Non-Newtonian fluids are also called nonlinear fluids as their rate of deformation and shear stress are not in a linear relationship. These fluids are present in the shape of toothpaste, paints, ketchup, and lubricants in our daily routine. Various fluidic models including Prandtl fluid, Prandtl–Eyring fluid, and power law fluid are some of those models that are scrutinized as viscoelastic fluidic models for their physical aspects. Munjam *et al.* [16] inspected MHD-PEFF (Prandtl–Eyring fluid flow) with convective heating over ST-S using the Keller–Box technique. Ullah *et al.* [17] used numerical treatment for PEFF under the effect of activation energy along ST-S.

Table 1
Physical parameters and their values involved in the MHD-PEFF model

Scenario 1	$\alpha = 3$	$\alpha = 4$	$\alpha = 5$	$\alpha = 6$
Scenario 2	$\beta = 0.01$	$\beta = 0.27$	$\beta = 0.54$	$\beta = 0.80$
Scenario 3	$M = 0.01$	$M = 0.6$	$M = 1.2$	$M = 1.8$

Shoaib *et al.* [18] examined PEFF in the form of a system of ordinary differential equations (ODEs) through a stochastic technique. Ullah *et al.* [19] theoretically analyzed PEFF involving nanoparticles in the form of a system of nonlinear ODEs using a Lobatto computational solver. Salawu *et al.* [20] investigated hydromagnetic PEFF using a semi-implicit difference technique. Shah *et al.* [21] discussed heat transfer phenomena to analyze engine oil-based PEFF with nanoparticles in hybrid form using the Chebyshev collocation method. Verma *et al.* [22] studied PEFF through a Darcy–Forchheimer medium in porous form using nanosized particles. Chaudhary *et al.* [23] scrutinized PEFF using Darcy–Forchheimer flow with Brownian diffusion effect containing nanoparticles. Some useful discussion about PEFF is presented in Refs. [24–26].

The stochastic techniques based on artificial neural networks (ANNs) have been implemented successfully in numerous daily life problems to solve them in the form of nonlinear ODEs for the last few decades due to their reliability and tendency to gain fast convergence. The applications of ANNs involved machine learning paradigms are computer virus treatment models [27,28], delay-based plant virus model [29], SIR model [30], laser transmission welding model [31], facial expression recognition [32], Lassa fever transmission model [33], Solar system [34], water production forecasting model [35], dish solar augmentation model [36],

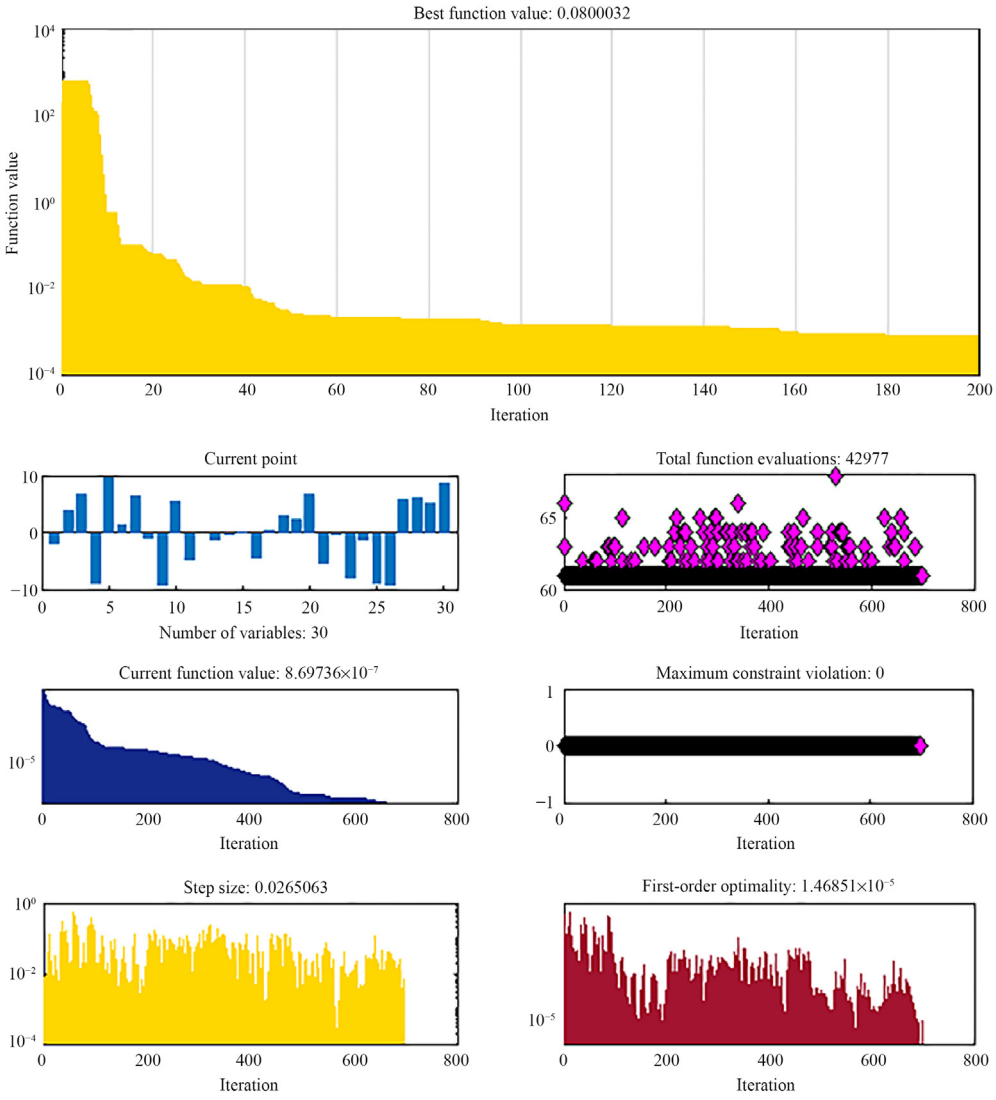

Fig. 2. Outcomes of PSO and SQP for optimizing the networks in scenario 1 (case 1) of MHD-PEFF problem.

spline model [37], corneal-shape paradigm [38], friction stir welding model [39], Casson fluid model [40], nanofluidic model [41], freshwater prediction model [42], model of induction motor [43,44], hybrid nanofluidic model [45], singularly perturbed delay differential equation and bio heat models [46–48], hybrid nanofluidic models [49,50], fin dynamical models [51,52], iterative malicious context learner in social networks [53], categorization of emotions in pets behavior [54], human action recognition in the video sequences [55], analysis of the prognosis system to predict employees job satisfaction [56], and implementation of multi-robotic navigation system [57]. These applications give a clear image of large-scale uses of ANNs, but the radial basis activation function (RBAF) currently involved to design computational algorithm in which particle swarm optimization (PSO) is involved, *i.e.* ANNs-RBAF-PSO solver, has never been used to analyze the MHD Prandtl–Eyring fluid flow (MHD-PEFF) model as per our literature survey. The highlights in terms of insights, contribution, and novelty of the current research study are briefly listed as follows:

- Hybridization of particle swarm optimization and sequential quadratic programming.
- Analysis of MHD-PEFF model *via* swarming intelligence-based ANNs-RBAF-PSO solver.
- Solution of MHD-PEFF model into a dimensionless form of third-order nonlinear ODE.
- Velocity analysis of the MHD-PEFF model *via* physical parameters-based scenarios.
- Graphical/tabulated form numerical results are verified *via* statistical analyses.

The further division of this research article is as follows. The second section is allocated for the formulation of the fluidic problem. The third section is assigned to present the methodology. Results and discussion are presented in Section 4 while Section 5 is for the conclusion.

2. Problem Formulation

Consider the two-dimensional incompressible steady-state PEFF along a stretchable sheet. The stretching of the sheet is linear (in the x-direction) while fluid is assumed to occupy in $y > 0$ direction. The magnetic field is applied with strength B acting perpendicular

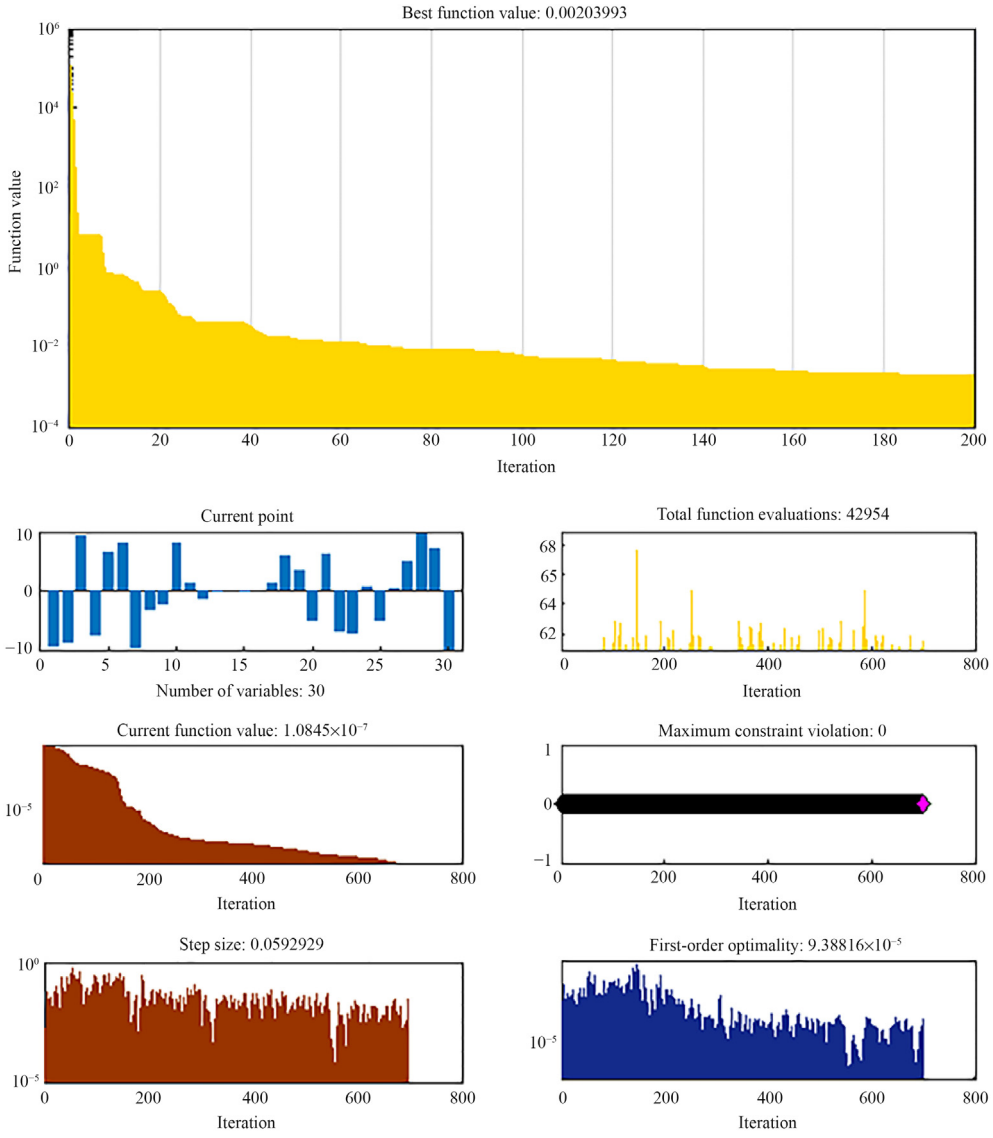

Fig. 3. Outcomes of PSO and SQP for optimizing the networks in scenario 2 (case 1) of MHD-PEFF problem.

to the direction of flow. The governing equations [58] are expressed as:

$$\frac{\partial u_1}{\partial x}+\frac{\partial u_2}{\partial y}=0 \tag{1}$$

$$u_1\frac{\partial u_1}{\partial x}+u_2\frac{\partial u_1}{\partial y}=\frac{A}{\rho_g C}\frac{\partial^2 u_1}{\partial y^2}-\frac{A}{2\rho_g C^3}\left(\frac{\partial u_1}{\partial y}\right)^2\frac{\partial^2 u_1}{\partial y^2}-\frac{\sigma_g {B_0}^2 u_1}{\rho_g} \tag{2}$$

Associated with boundary conditions.

$$\begin{aligned} &u_1=U=a_1x, u_2=0 \quad \text{at} \quad y=0\\ &u_1\to 0 \quad \text{at} \quad y\to\infty \end{aligned} \tag{3}$$

The form of the stream function is:

$$u_1=\frac{\partial\psi}{\partial y}, u_2=-\frac{\partial\psi}{\partial x} \tag{4}$$

The similarity transformation used here:

$$\eta=\left(\frac{a_1}{\nu_g}\right)^{\frac{1}{2}}y, \psi=\left(\nu_g a_1\right)^{\frac{1}{2}}x\, g(\eta) \tag{5}$$

Substitution of Eq. (5) into Eqs. (1)–(3) generates.

$$\alpha g'''(\eta)-\alpha\beta(g''(\eta))^2 g'''(\eta)-(g'(\eta))^2+g(\eta)g''(\eta)-Mg'(\eta)=0 \tag{6}$$

With boundary conditions

$$g(0)=0, g'(0)=1, g'(\infty)=0 \tag{7}$$

The dimensionless parameters involved in Eq. (6) are formulated as:

$$M=\frac{\sigma_g B^2}{a\rho_g}, \alpha=\frac{A}{\mu_g C}, \beta=\frac{a^3x^2}{2C^2\nu_g} \tag{8}$$

3. Methodology

The assumed numerical solution formulation using ANNs-RBAF-PSO solver is:

$$\widehat{g}(\eta)=\sum_{k=1}^{n} m_{1k}F(m_{2k}\eta+m_{3k}) \tag{9}$$

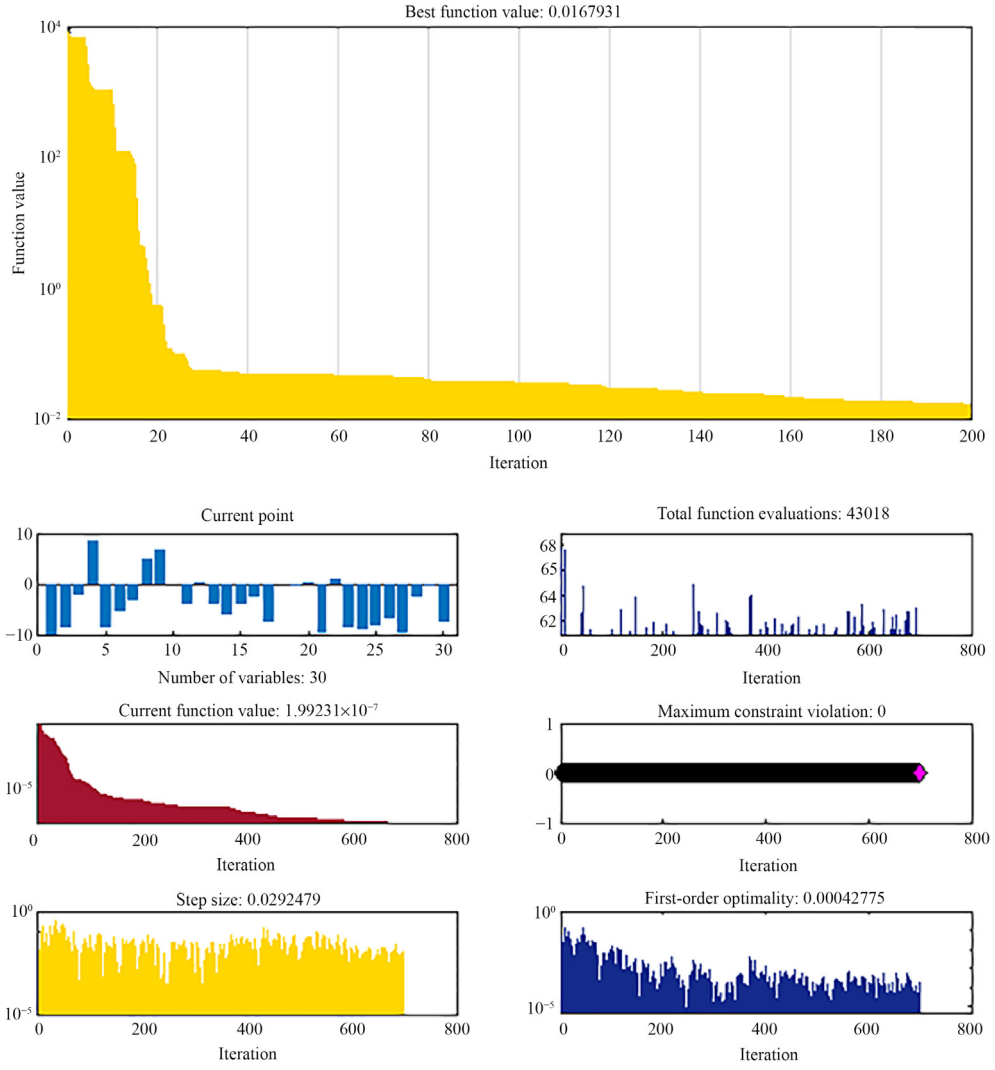

Fig. 4. Outcomes of PSO and SQP for optimizing the networks in scenario 3 (case 1) of MHD-PEFF problem.

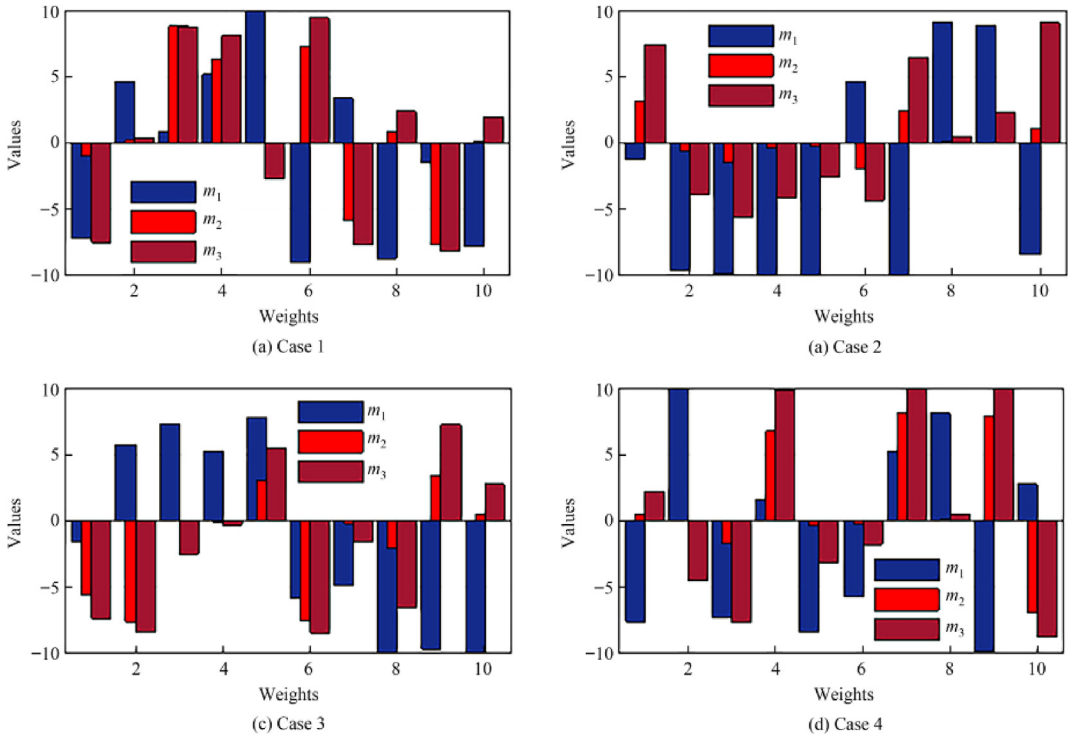

Fig. 5. Weights calculated in first scenario of MHD-PEFF problem using ANNs-RBAF-PSO solver.

$$\widehat{g}^{(j)}(\eta) = \sum_{k=1}^{n} m_{1k} F^{(j)}(m_{2k}\eta + m_{3k}) \tag{10}$$

The form of targeted weights used in the current research is $W = [m_1, m_2, m_3]$ while $F(x) = 1/\sqrt{1+x^2}$ is the radial basis activation function used in ANNs-RBAF-PSO solver. So, the transformed form of Eq. (9) along the involved highest order derivative is:

$$\widehat{g}(\eta) = \sum_{k=1}^{n} \frac{m_{1k}}{\sqrt{1+(m_{2k}\eta + m_{3k})^2}} \tag{11}$$

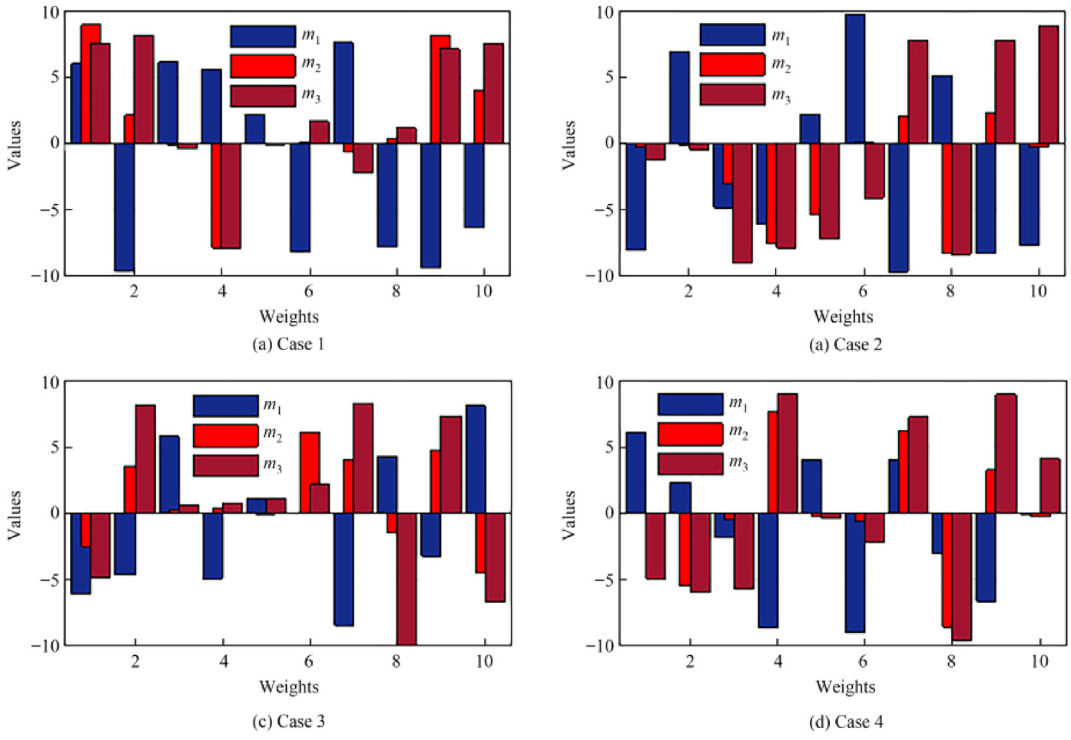

Fig. 6. Weights calculated in second scenario of MHD-PEFF problem using ANNs-RBAF-PSO solver.

$$\widehat{g'''}(\eta)=\sum_{k=1}^{n}\left[m_{1k}m_{2k}^{3}\left(\frac{9(m_{2k}\eta+m_{3k})}{\left(1+(m_{2k}\eta+m_{3k})^{2}\right)^{5/2}}-\frac{15(m_{2k}\eta+m_{3k})^{3}}{\left(1+(m_{2k}\eta+m_{3k})^{2}\right)^{7/2}}\right)\right] \tag{12}$$

Fig. 1(a) shows the hierarchical structure of the design solver, which provides a visual representation of its architecture designed to solve the suggested problem. The ANN-RBAF-PSO solver used to solve the fluid model of the faceplate consists of three layers: an input layer, a hidden layer, and an output layer. The input layer serves to represent the inputs, while the hidden layer contains activation functions critical for neurons and actions. The output layer performs the rest of the calculations, representing the final stage of the solver's structure diagram.

The fitness function formulation for nonlinear ODE with associated boundary equations is presented in Eqs. (6) and (7) is:

$$E_{11}=\frac{1}{r}\sum_{s=1}^{r}\left(\alpha\widehat{g'''}_{s}(\eta)-\alpha\beta(\widehat{g''}_{s}(\eta))^{2}\widehat{g'''}_{s}(\eta)-(\widehat{g'}_{s}(\eta))^{2}+\widehat{g}_{s}(\eta)\widehat{g''}_{s}(\eta)-M\widehat{g'}_{s}(\eta)\right)^{2} \tag{13}$$

$$E_{22}=\frac{1}{3}\left[(\widehat{g}_{1})^{2}+(\widehat{g}_{1}{}'-1)^{2}+\widehat{g'}_{q}{}^{2}\right] \tag{14}$$

$$E_{0}=E_{11}+E_{22} \tag{15}$$

For optimization, the fitness function E_0 should approach nearly equal zero.

The training of weights involved in Eqs. (6) and (7) are performed using the amalgam of PSO with SQP. The details of this learning process are presented as:

Algorithm 1
Pseudocode constructed through ANNs-RBAF-PSO solver for MHD-PEFF problem

Global search stage
PSO (Start*)
Initialization: Adjustment through parameters of PSO as well as optimization after the formation of randomly generated swarm.
Termination: Process stops if anyone given below achieved.
- Swarmsize ↔ 200
- Other settings (default*)

Fitness estimation: Each involved particle in Eqs. (6) and (7) is scrutinized for fitness check ($\boldsymbol{E_0}$).
Ranking: Rank the minimum fitness level of $\boldsymbol{E_0}$ with each particle.
Stopping criteria: Process stops when the best fitness level is attained and desired cycles/flights achieved.
Renewal: Alteration in position/velocity through Eqs. (16) and (17).
Upgrade: Adjustments in fitness for gaining all flights.
Storage: Store best-calculated global values as well as fitness.
PSO(End*)
Local search stage
Hybrid PSO-SQP(Start*)
Inputs: PSO best outcomes.
Output: Best trained weights *i.e.* $\boldsymbol{W_{B\text{-}PSOSQP}}$.
Initialize: Utilize the Global Solver best values as a "start point".
Termination: Process stops if anyone is attained.
- "MaxFun ↔ 100000", "TolCon ↔ 1 × 10^{-15}", "MaxIter ↔ 700", "TolX ↔ 1 × 10^{-20}"
- Other (by default*)

Fitness estimation: Calculate $\boldsymbol{E_0}$ using Eq. (15).
Adjustment: Adjustment *via* "fmincon" for $\boldsymbol{W_{B\text{-}PSOSQP}}$.
Store: Collection of $\boldsymbol{W_{B\text{-}PSOSQP}}$ and $\boldsymbol{E_0}$.
Hybrid PSO-SQP(End*)

(1) Particle swarm optimization (PSO)

The swarm intelligence-based algorithms are called PSO algorithms which were introduced by Eberhart and Kennedy [59], Ahmad *et al.* [60], and Rangasamy *et al.* [61]. The "fish schooling" as well as the "bird flocking" are those models that are behind the

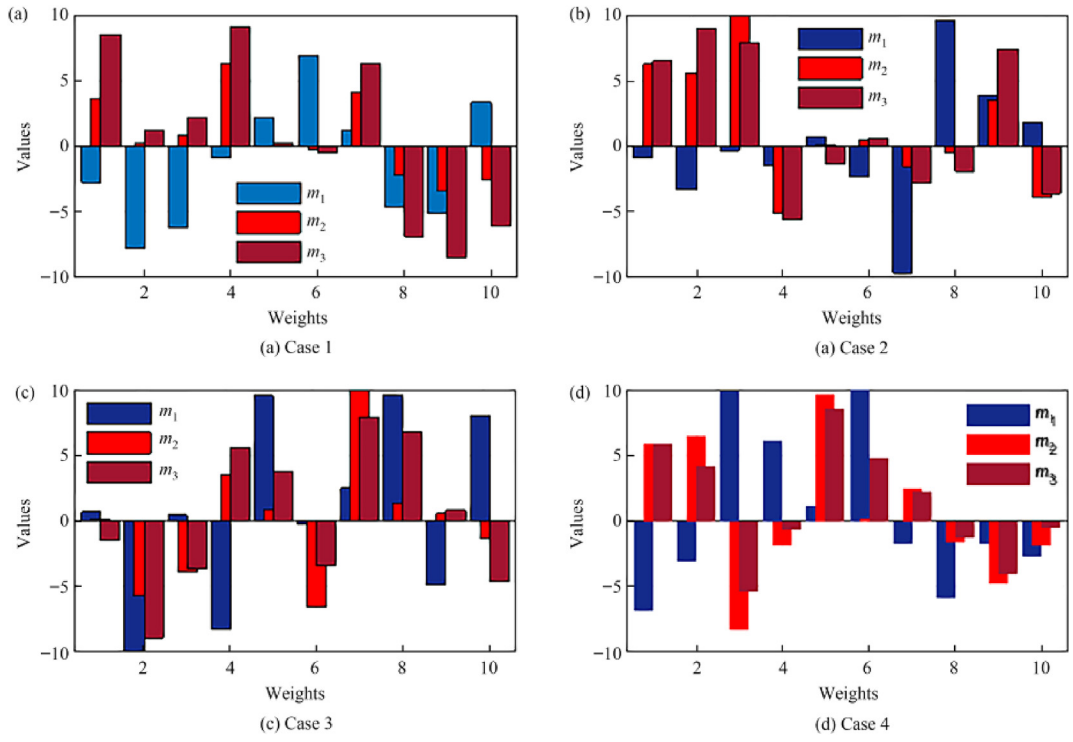

Fig. 7. Weights calculated in the third scenario of the MHD-PEFF problem using ANNs-RBAF-PSO solver.

development of this global searching method through inspiration based on social behavior. The algorithms based on PSO are constructed through a class of particles called "swarm" where the velocity and position are represented by V and S respectively and are modified on this basis of Q_{p-1}^{LB} which is the previous best "local position" of all actively involved particles Q_{p-1}^{LB} in a swarm. The formulation of V and S are:

$$V_p^n = \omega V_{p-1}^n + d_1 R_1 \left(Q_{p-1}^{LB} - X_{q-1}^n\right) + d_2 R_2 \left(Q_{p-1}^{GB} - X_{p-1}^n\right) \quad (16)$$

$$X_p^n = X_{p-1}^n + V_p^n \quad (17)$$

Here V^n represents the "nth particle" velocity and X^n is its vectorial form in a swarm. The maximum velocity is represented by V_{max} while $V_p \in [-V_{max}, V_{max}]$, d_1 and d_2 are expressed global local form constants for acceleration, R_1 and R_2 represent vectors having elements distribution in "0 to 1" while ω representing inertia weight with a tendency to depreciate linearly. Some recent PSO-based applications are the solution of biological nonlinear Leptospirosis systems [62,63], autoregressive systems [64], and parameter estimation of the harmonics in electrical systems [65].

(2) Sequential quadratic programming (SQP)

The hybridization of PSO with some local search solver enhances its tendency to gain a rapid convergence in case of nonlinear ODEs and for this purpose, SQP is used in the current research. SQP is an

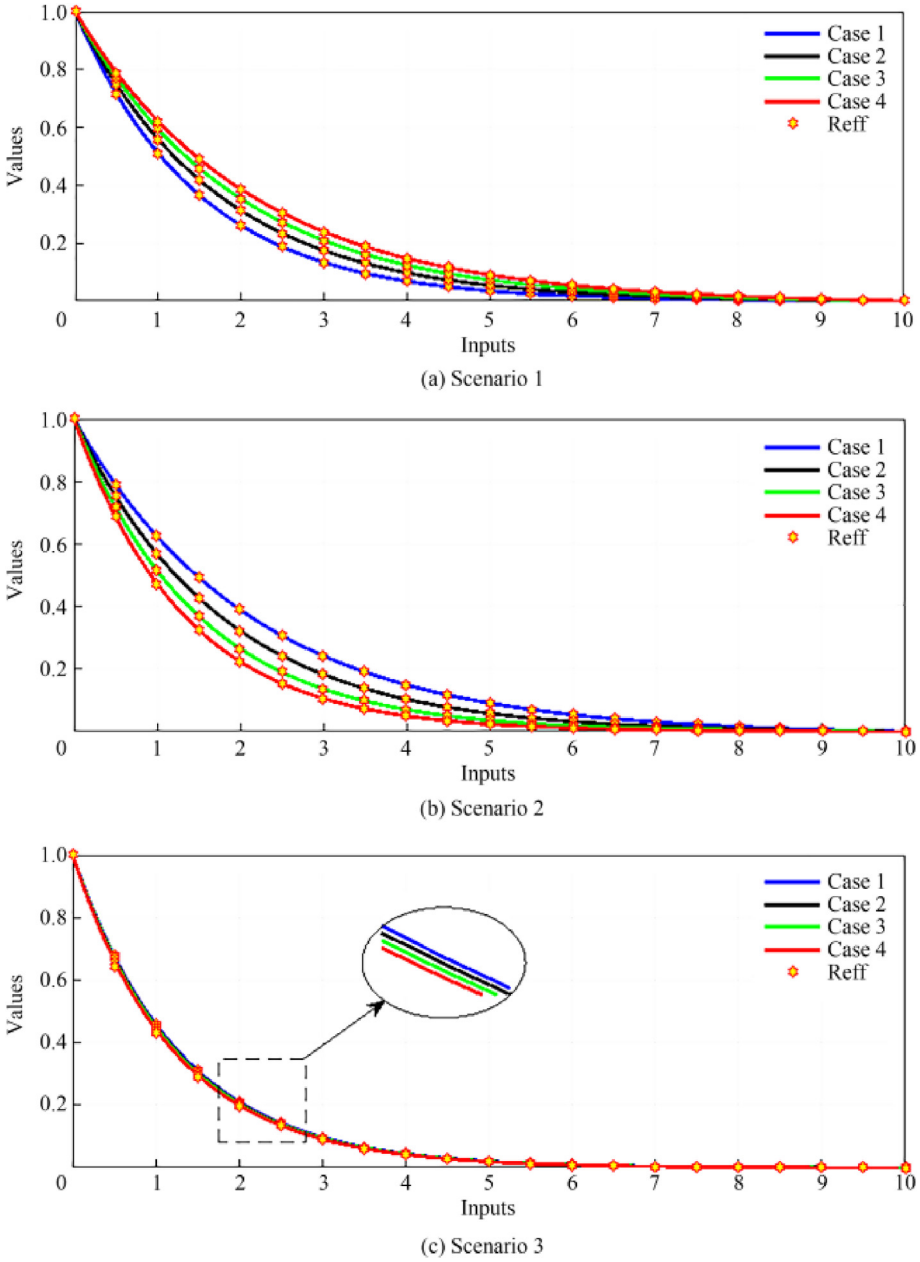

Fig. 8. Numerical values of $\ddot{g}'(\eta)$ calculated in 1–3 scenarios of MHD-PEFF problem.

efficient local solver introduced in the '90s [66] and is known as a "nonlinear programming technique". Some purposeful applications based on SQP are analysis of the tuberculosis model [67], Casson nanofluidic model [68], analysis of MHD nanofluid boundary layer flow system [69], electro-magnetohydrodynamic effects on Darrcy–Forchheimer viscous fluid flow model [70]. Algorithm 1 is the presentation of the pseudocode of the ANNs-RBAF-PSO algorithm while Fig. 1(b) represents its flowchart.

(3) Performance metric

The efficacy of the proposed ANNs-RBAF-PSO solver is scrutinized using various statistical performance-based operators having formulations as:

$$\begin{aligned}
\mathrm{RMSE}_{\hat{g}} &= \sqrt{\frac{1}{k}\sum_{l=1}^{k}\left(\widehat{g}_l - g_{\mathrm{ref}:l}\right)^2},\\
\mathrm{NSE}_{\hat{g}} &= 1 - \frac{\sum_{l=1}^{k}\left(\widehat{g}_l - g_{\mathrm{ref}:l}\right)^2}{\sum_{l=1}^{k}\left(\widehat{g}_l - \overline{g_q}\right)^2},\\
\mathrm{VAF}_{\hat{g}} &= \left(1 - \frac{\mathrm{var}\left(g_{\mathrm{ref}:l} - \widehat{g}_l\right)}{\mathrm{var}(g_l)}\right) \times 100
\end{aligned} \tag{18}$$

RMSE means root mean square error), VAF is variance accounted for, NSE is nash-sutcliffe-efficiency.

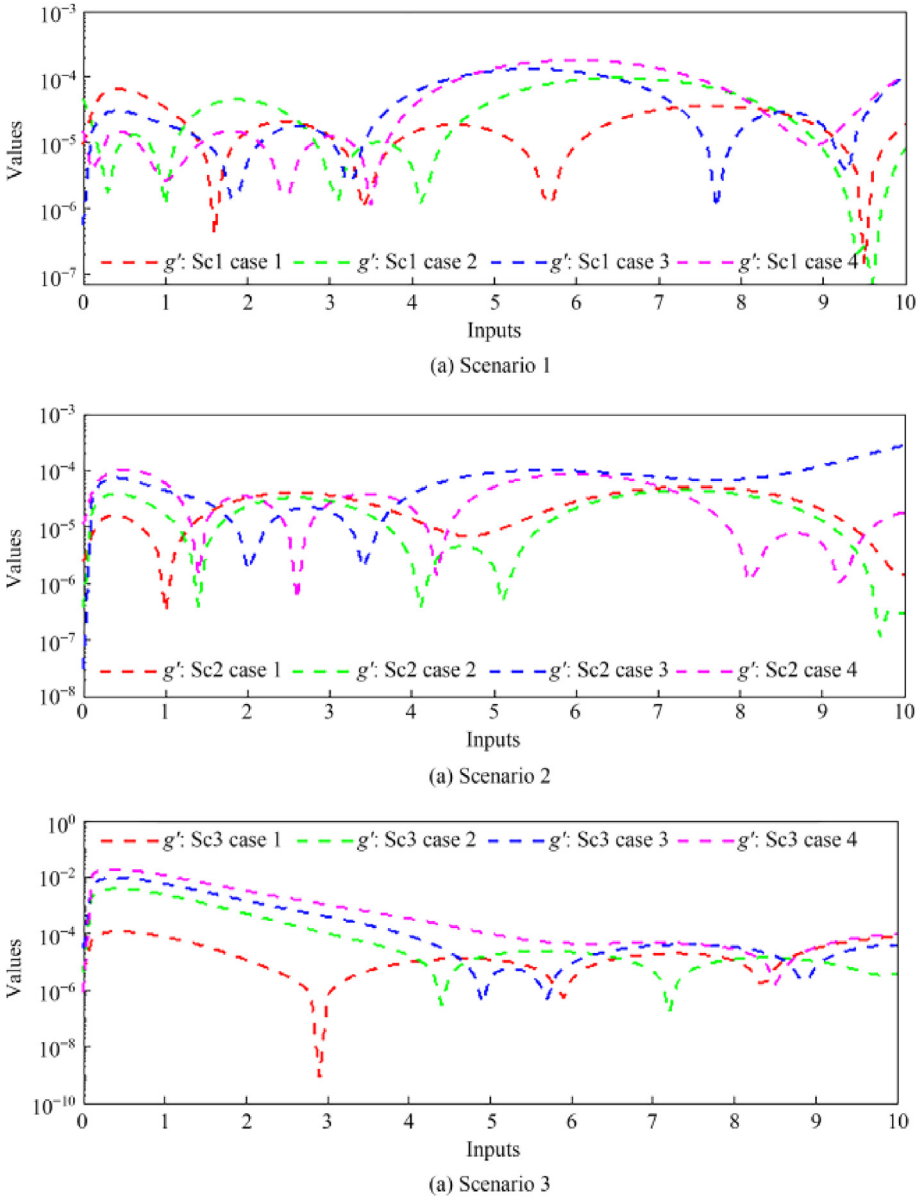

Fig. 9. AEs in $\hat{g}'(\eta)$ using ANNs-RBAF-PSO solver in scenarios 1–3 of MHD-PEFF problem.

$$
\begin{aligned}
&E-\mathrm{VAF}_{\hat{g}}=100-\mathrm{VAF}_{\hat{g}},\\
R_{\hat{g}}{}^2=\frac{SS_{\mathrm{reg}:\hat{g}}}{SS_{\mathrm{total}:\hat{g}}},\ &E-R_{\hat{g}}{}^2=1-R_{\hat{g}}{}^2,\\
&E-\mathrm{NSE}_{\hat{g}}=1-\mathrm{NSE}_{\hat{g}},\\
&\mathrm{MAE}_{\hat{g}}=\sum_{l=1}^{k}\left|\hat{g}_l-g_{\mathrm{ref}:l}\right|,\\
\mathrm{TIC}_{\hat{g}}=&\frac{\sqrt{\frac{1}{k}\sum_{l=1}^{k}\left(\hat{g}_l-g_{\mathrm{ref}:l}\right)^2}}{\sqrt{\frac{1}{k}\sum_{l=1}^{k}\hat{g}_l{}^2}+\sqrt{\frac{1}{k}\sum_{l=1}^{k}g_{\mathrm{ref}:l}^2}}
\end{aligned}
\tag{19}
$$

MAE is mean-absolute-error and TIC is Theil's-inequality-coefficient.

The effectiveness of the designed ANNs-RBAF-PSO solver is guaranteed if the obtained results using these operators are very close to zero.

4. Results and Discussion

The newly designed ANNs-RBAF-PSO solver is used to analyze MHD-PEFF model along a stretching sheet with an amalgam of PSO-SQP solver on the interval [0,10]. The current problem is solved for three scenarios which are constructed using physical parameters that exist in MHD-PEFF problem and the values assigned are presented in Table 1.

The weights attached with the assumed numerical solution of MHD-PEFF problem are trained through the designed algorithm and the learning curves obtained during this process of obtaining

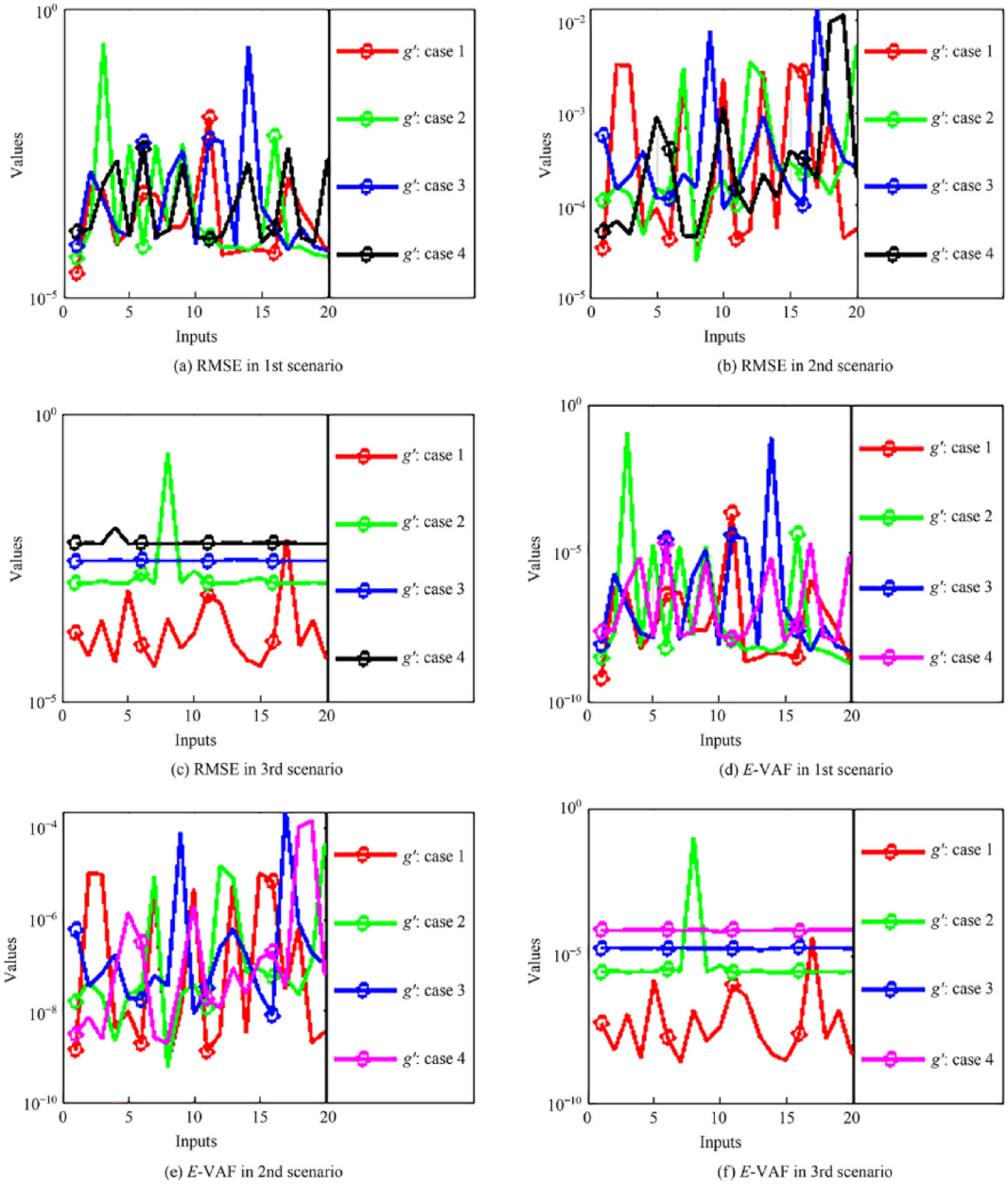

Fig. 10. RMSE and *E*-VAF analyses in all three scenarios of MHD-PEFF problem.

the best weights in first case of all scenarios are depicted in Figs. 2–4.

It indicates that the accuracy of the ANNs-RBAF-PSO solver uplifts through the hybridization of PSO with SQP also the best-obtained weights in all three scenarios are illustrated in Figs. 5–7. The substitution of these weights in Eq. (6) gives the required numerical outcomes of MHD-PEFF problem using ANNs-RBAF-PSO solver. The numerical values obtained for velocity $\hat{g}'(\eta)$ in all three scenarios using the suggested solver are presented through graphs in Figs. 8–10 and successfully match with the reference solution which proves that the designed scheme is suitable to solve MHD-PEFF problem. Fig. 8(a) represents the effect of Prandtl–Eyring fluid parameter α on $\hat{g}'(\eta)$. A larger value of α in the Prandtl–Eyring fluid model induces a stronger shear-thinning behavior and lowers the viscosity at higher shear rates. This reduced resistance to flow near surfaces leads to increased fluid velocity, especially in boundary layers or near obstacles. Higher values of α promote better shear thinning and reduced flow resistance, which ultimately increases the fluid velocity in Prandtl–Eyring fluids.

Fig. 8(b) displays the impact of fluid parameter β on $\hat{g}'(\eta)$. The expanded value of β mitigates the momentum diffusivity. This reduction in momentum diffusivity means a reduction in the fluid's ability to transfer momentum through flow. Consequently, the fluid experiences greater resistance to flow and exhibits a lower velocity as β increases. The relationship between β and momentum diffusivity highlights how changes in fluid viscosity affect the overall flow dynamics, with higher values of beta leading to reduced momentum transfer and reduced fluid velocity. Fig. 8(c) depicts the consequences of Hartmann number M on $\hat{g}'(\eta)$. As the value of M increases in MHD flow, stronger electromagnetic forces relative to viscous forces dampen the fluid motion. This damping effect is

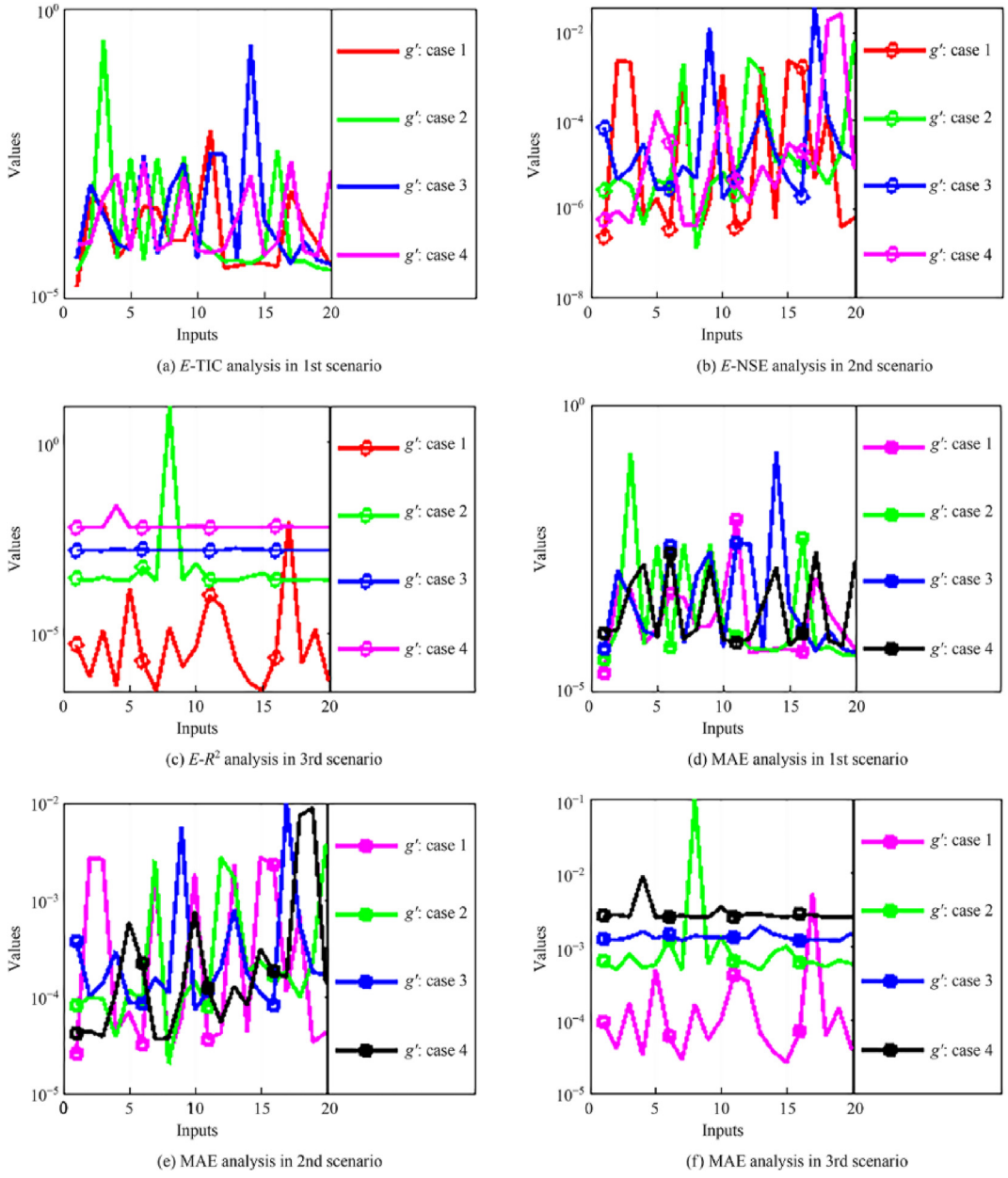

Fig. 11. Analyses of randomly taken scenarios for the MHD-PEFF problem using multiple operators.

Table 2
AEs in $\hat{g}'(\eta)$ using S-(I–IV) of MHD-PEFF problem

H	C-1	C-2	C-3	C-4
Scenario 1 (S-1)				
0	1.295473×10^{-4}	4.085982×10^{-2}	3.538054×10^{-2}	1.462229×10^{-4}
1	6.691958×10^{-5}	2.427739×10^{-2}	2.234821×10^{-2}	3.572841×10^{-5}
2	3.036911×10^{-4}	1.407190×10^{-2}	1.312198×10^{-2}	3.486039×10^{-5}
3	5.876590×10^{-4}	8.550118×10^{-3}	7.479969×10^{-3}	3.369687×10^{-4}
4	4.657344×10^{-4}	5.409650×10^{-3}	4.023716×10^{-3}	7.598405×10^{-4}
5	3.520841×10^{-4}	3.256564×10^{-3}	1.439186×10^{-3}	8.300386×10^{-4}
6	7.599237×10^{-4}	1.570647×10^{-3}	1.804827×10^{-3}	4.719398×10^{-4}
7	1.242663×10^{-3}	7.922307×10^{-4}	3.247671×10^{-3}	4.002825×10^{-4}
8	1.481238×10^{-3}	1.142384×10^{-3}	4.985832×10^{-3}	1.088453×10^{-3}
9	1.446536×10^{-3}	1.642584×10^{-3}	6.775412×10^{-3}	1.727119×10^{-3}
10	1.419959×10^{-3}	2.231675×10^{-3}	8.622495×10^{-3}	2.388700×10^{-3}
S-2				
0	2.091172×10^{-4}	1.397515×10^{-4}	2.441759×10^{-4}	4.140514×10^{-4}
1	1.140777×10^{-4}	7.312554×10^{-5}	1.002479×10^{-4}	1.496674×10^{-4}
2	3.021438×10^{-4}	1.832362×10^{-4}	2.604078×10^{-4}	3.888882×10^{-4}
3	7.848486×10^{-4}	4.981307×10^{-4}	6.074068×10^{-4}	8.280860×10^{-4}
4	1.416942×10^{-3}	8.113254×10^{-4}	5.206920×10^{-4}	5.907156×10^{-4}
5	1.659139×10^{-3}	6.997001×10^{-4}	4.536656×10^{-4}	2.058870×10^{-4}
6	1.346699×10^{-3}	4.017320×10^{-4}	8.861588×10^{-4}	8.319599×10^{-4}
7	6.436929×10^{-4}	5.113958×10^{-4}	1.403481×10^{-3}	1.330550×10^{-3}
8	4.517036×10^{-4}	9.619619×10^{-4}	1.790918×10^{-3}	1.707223×10^{-3}
9	1.309850×10^{-3}	1.358643×10^{-3}	2.313795×10^{-3}	2.248037×10^{-3}
10	2.128928×10^{-3}	1.879587×10^{-3}	2.935816×10^{-3}	2.852100×10^{-3}
S-3				
0	2.887644×10^{-4}	4.108060×10^{-2}	5.753886×10^{-5}	6.142620×10^{-4}
1	1.350743×10^{-4}	2.076154×10^{-2}	5.923104×10^{-3}	1.132700×10^{-2}
2	9.326009×10^{-5}	8.616046×10^{-3}	1.479845×10^{-3}	3.502449×10^{-3}
3	3.233601×10^{-4}	3.610092×10^{-3}	4.753209×10^{-4}	1.552290×10^{-3}
4	3.250364×10^{-4}	1.358698×10^{-3}	1.780387×10^{-4}	7.029578×10^{-4}
5	1.516484×10^{-4}	4.278096×10^{-4}	8.065423×10^{-5}	1.328357×10^{-4}
6	1.786388×10^{-4}	2.410369×10^{-4}	1.300656×10^{-4}	4.235418×10^{-4}
7	3.629637×10^{-4}	3.191503×10^{-4}	1.015203×10^{-4}	6.536452×10^{-4}
8	5.952035×10^{-4}	4.428220×10^{-4}	1.893243×10^{-4}	9.035940×10^{-4}
9	9.280542×10^{-4}	8.614020×10^{-4}	4.906781×10^{-4}	1.336032×10^{-3}
10	1.343286×10^{-3}	1.476283×10^{-3}	9.806919×10^{-4}	1.915607×10^{-3}

caused by the Lorentz force, which acts against the flow of fluid in the presence of a magnetic field. Consequently, higher values of M lead to greater resistance to fluid motion and lower fluid velocity. This decrease in velocity occurs due to the damping effect of electromagnetic forces that act against the flow of the fluid and restrict its movement. Taken together, the impact of M on fluid velocity underscores the complex balance between electromagnetic and viscous forces in magnetohydrodynamic systems.

Moreover, the obtained numerical outcomes are executed to calculate absolute errors (AEs) and Fig. 9 illustrates the AEs

Table 3
Best-obtained iterations in $\hat{g}'(\eta)$ using all scenarios of MHD-PEFF model

Operators	Numerical value (N. value)	It#	N. value	It#	N. value	It#	N. value	It#
Scenario 1 (S-1)								
E-R^2	6.800929×10^{-4}	1	1.751271×10^{-5}	1	2.092012×10^{-4}	20	1.274762×10^{-5}	19
RMSE	1.834883×10^{-3}	1	2.944428×10^{-4}	1	1.017669×10^{-3}	20	2.512111×10^{-4}	19
MAE	1.319998×10^{-3}	1	2.510188×10^{-4}	1	8.100934×10^{-4}	20	2.010310×10^{-4}	19
E-TIC	2.593840×10^{-3}	1	4.163979×10^{-4}	1	1.439053×10^{-3}	20	3.552659×10^{-4}	19
E-NSE	6.800929×10^{-4}	1	1.751271×10^{-5}	1	2.092012×10^{-4}	20	1.274762×10^{-5}	19
E-VAF	3.281289×10^{-6}	1	4.784605×10^{-8}	20	7.663848×10^{-7}	17	4.584097×10^{-8}	19
S-2								
E-R^2	3.158780×10^{-4}	8	1.518531×10^{-6}	8	1.046678×10^{-5}	10	1.759751×10^{-6}	8
RMSE	1.250501×10^{-3}	8	8.670341×10^{-5}	8	2.276307×10^{-4}	10	9.333615×10^{-5}	8
MAE	9.400085×10^{-4}	8	7.439381×10^{-5}	8	1.861605×10^{-4}	10	8.377114×10^{-5}	7
E-TIC	1.768369×10^{-3}	8	1.226165×10^{-4}	8	3.218750×10^{-4}	10	1.319959×10^{-4}	8
E-NSE	3.158780×10^{-4}	8	1.518531×10^{-6}	8	1.046678×10^{-5}	10	1.759751×10^{-6}	8
E-VAF	1.373876×10^{-6}	8	4.005743×10^{-9}	8	3.466320×10^{-8}	16	3.421948×10^{-9}	8
S-3								
E-R^2	2.138225×10^{-4}	7	3.747551×10^{-6}	4	1.431722×10^{-4}	3	1.315223×10^{-6}	7
RMSE	1.028848×10^{-3}	7	1.362066×10^{-4}	4	8.414618×10^{-4}	3	8.065006×10^{-5}	7
MAE	6.517399×10^{-4}	15	1.133212×10^{-4}	13	6.819491×10^{-4}	16	6.642514×10^{-5}	9
E-TIC	1.455004×10^{-3}	7	1.926252×10^{-4}	4	5.053357×10^{-4}	3	4.844672×10^{-5}	7
E-NSE	2.138225×10^{-4}	7	3.747551×10^{-6}	4	1.431722×10^{-4}	3	1.315223×10^{-6}	7
E-VAF	1.280200×10^{-6}	7	1.153528×10^{-8}	14	6.984414×10^{-7}	13	6.013216×10^{-9}	10

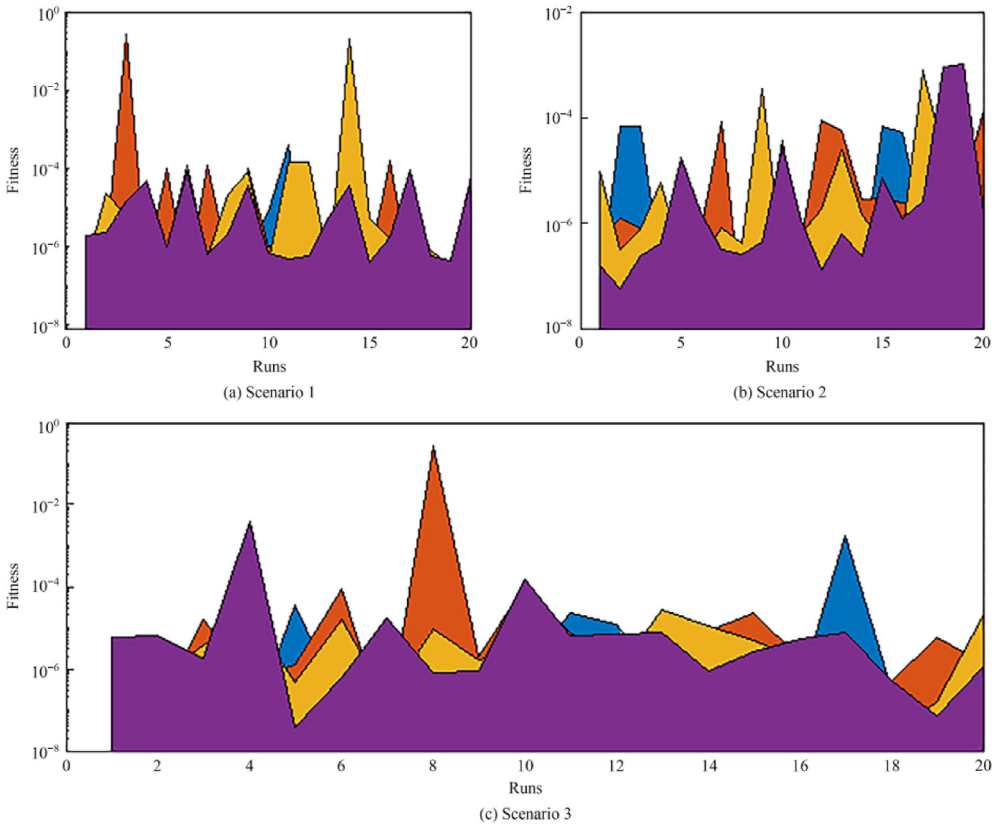

Fig. 12. Fitness in terms of area calculated in all three scenarios of MHD-PEFF problem.

graphs acquired in scenarios 1–3 of the proposed problem and depicts that the range of accuracy calculated in the first scenario lies in a range from 10^{-3} to 10^{-7} (up to 6 decimal places), for the second scenario this range is from 10^{-3} to 10^{-8} and in the third scenario this range lies from 10^{0} to 10^{-10}. The achieved exceptional accuracy with AEs calculated to nine decimal places highlights the robustness of our methodology. These findings confirm the effectiveness of our technique in accurately capturing complex fluid flow dynamics. Furthermore, the remarkable accuracy achieved underlines the suitability of our methodology for various computational fluid dynamics applications.

The stability and efficiency of the designed ANNs-RBAF-PSO solver are comprehensively determined through various convergence and fitness analyses using some well-known statistical operators. Fig. 10 represents RMSE and *E*-VAF analyses in all three scenarios of the MHD-PEFF problem and respectively lie in a range up to 10^{-5} and 10^{-10}. Fig. 11 illustrates *E*-TIC, *E*-NSE, and MAE in randomly selected scenarios and lies in a range up to 10^{-5}. The obtained results confirm that the designed solver can handle stiff nonlinear problems like the MHD-PEFF model quite effectively. Achieving accuracy to nine decimal places across various performance operators underscores its expertise in capturing complex fluid dynamics phenomena. The consistent

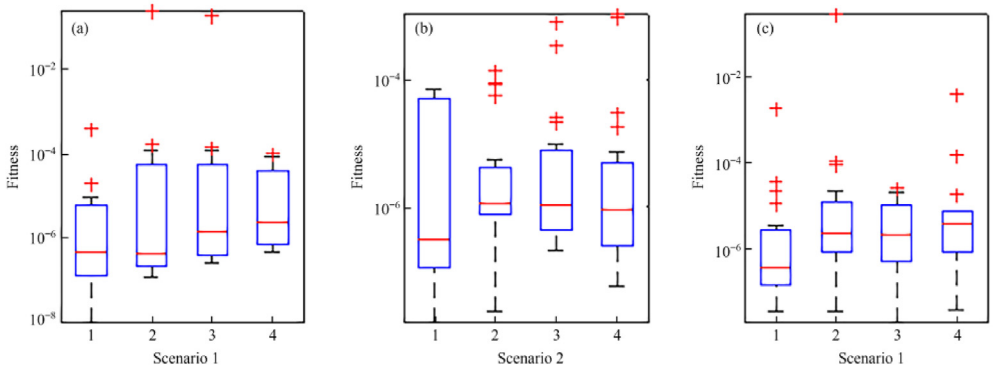

Fig. 13. Fitness in terms of boxplot analysis in all three scenarios of MHD-PEFF model.

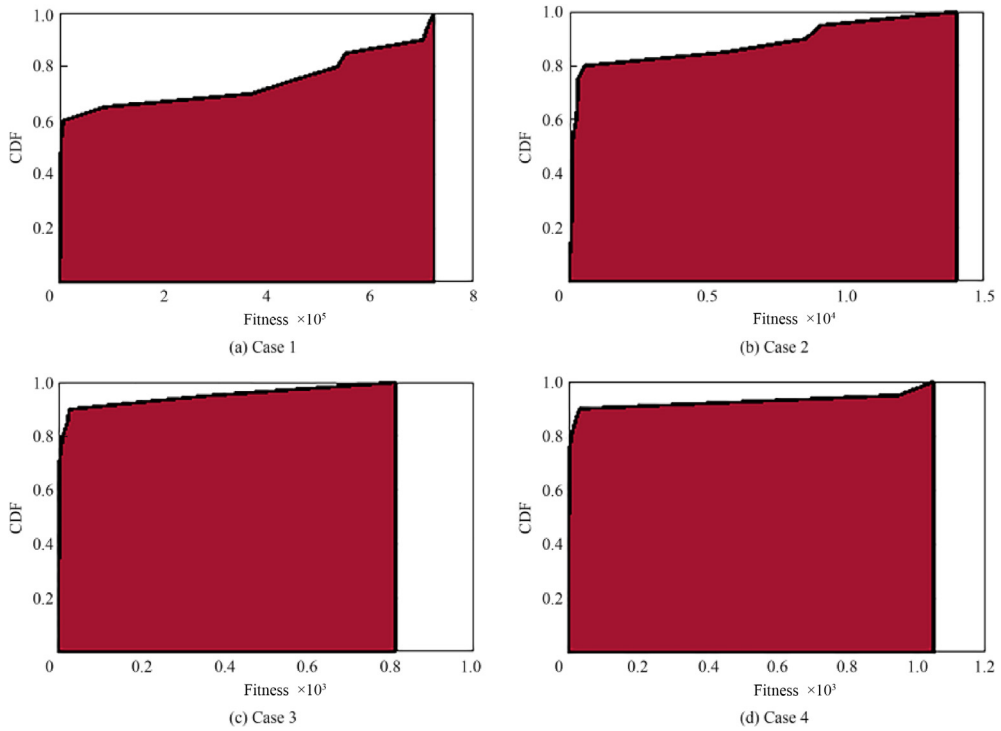

Fig. 14. Fitness in terms of CDF analysis in second scenarios of MHD-PEFF problem.

stability and reliability demonstrated by our solver highlight its effectiveness in providing accurate solutions for the suggested problem. These findings confirm that the design solver is an excellent choice. The best values calculated through various statistical operators along the obtained iteration number (It #) are depicted in Tables 2 and 3.

The fitness of the proposed ANNs-RBAF-PSO solver is scrutinized in terms of area, CDF (cumulative distributive function), Boxplot, and

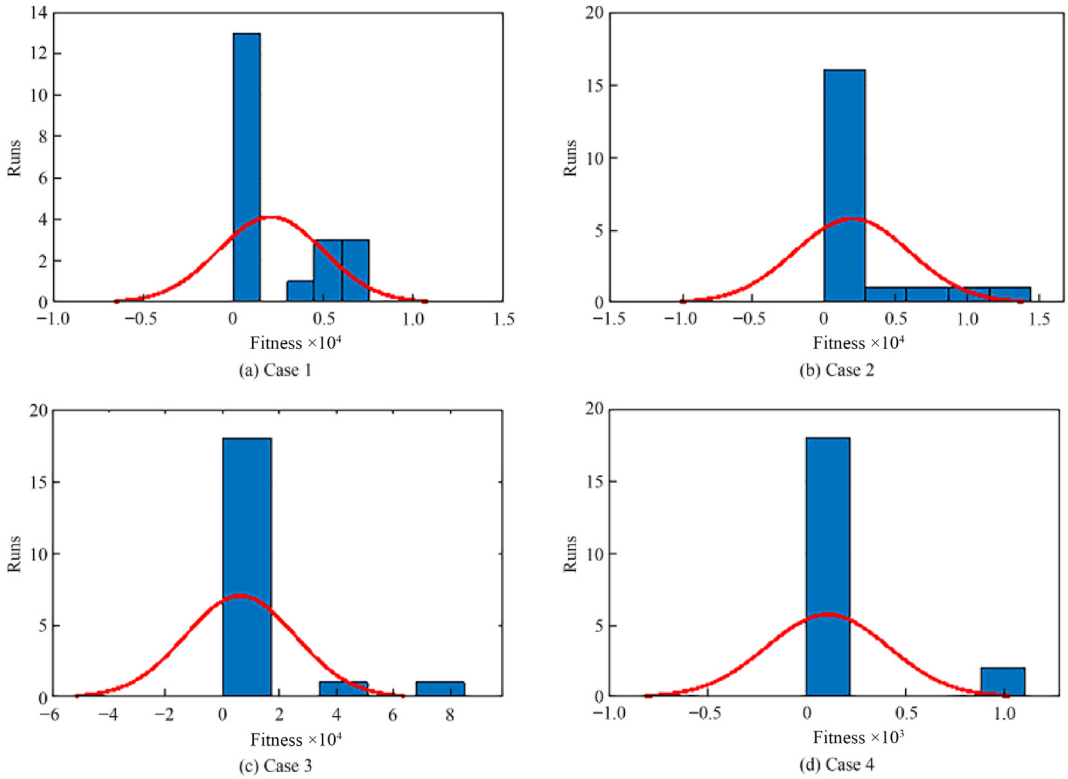

Fig. 15. Fitness in terms of histogram analysis in second scenario of MHD-PEFF problem.

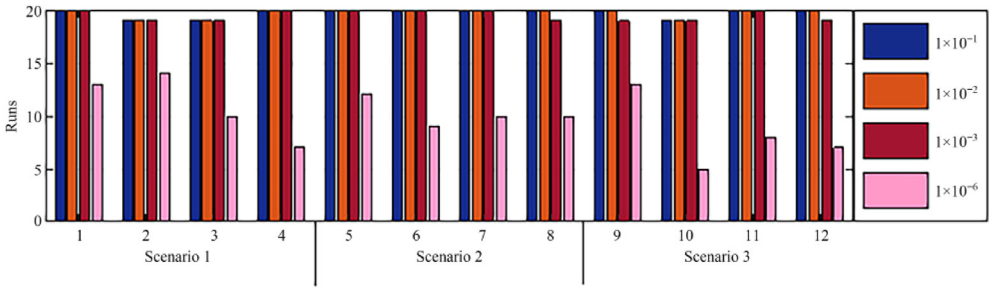

Fig. 16. Convergence analysis in terms of fitness in all three scenarios of MHD-PEFF problem.

Histogram analyses. Fig. 12 represents fitness in terms of area for all scenarios of the MHD-PEFF problem lie a range of accuracy up to 10^{-9}. Fig. 13 illustrates the boxplot analysis and range of accuracy for first, second and third scenarios is 10^{-2} –10^{-8}, 10^{-4} –$10^{-7,}$ and 10^{-2} –10^{-7} respectively. Such high accuracy indicates that the solver effectively minimizes errors and ensures that the predicted velocity profiles closely match the actual behavior of the fluid flow and also demonstrates the solver's effectiveness in minimizing deviations from actual fluid behavior, providing confidence in model predictions and ensuring reliable analysis of fluid flow under varying magnetic and fluid parameters. Fig. 14 shows the CDF analysis for fitness evaluation of the designed solver in all cases of the second scenario and the achieved precision consistently falls within a continuum of 10^{-3} –10^{-5}. Fig. 15 depicts an analysis in terms of histograms in cases 1–4 of the second scenario and the accuracy range is 10^{-3} –10^{-4}. This level of accuracy reflects the solver's effectiveness in capturing subtle changes in fluid flow, ensuring that numerical solutions closely match the expected physical phenomena. In the context of a PEFF model using ANN's-RBAF-PSO technique, these histogram results highlight the robust performance of the solver. The hybridization of PSO and SQP allows the solver to efficiently handle the complexities of nonlinear fluid dynamics problems. Histogram analysis supports the conclusion that the solver provides a consistent and accurate representation of fluid flow, which is crucial for applications where accuracy is critical. Fig. 16 shows the convergence analysis for the fitness obtained in all three scenarios of the MHD-PEFF problem and indicates that almost 60% of runs attain a stiff criterion of accuracy up to 10^{-6} (5 decimal places).

This comprehensive fitness analysis strongly recommends the newly designed ANNs-RBAF-PSO solver is suitable for the dynamical analysis of the MHD-PEFF problem.

5. Conclusions

A newly designed ANNs-RBAF-PSO solver is constructed to analyze the MHD-PEFF model along a stretched sheet. The velocity profile $\hat{g}'(\eta)$ is computed by varying three existing parameters in the suggested problem. The calculated AEs obtained an accuracy of up to 9 decimal places which is a manifestation of highly accurate numerical outcomes. The accuracy of ANNs-RBAF-PSO solver is obtained in terms of various statistical operators which lies in a range of 4 ↔ 9 decimal places which clearly shows the stability of the designed scheme. The principal outcome is Velocity $\hat{g}'(\eta)$ escalates with a larger value of the Prandtl–Eyring fluid parameter α as a higher value of α reduces the fluid viscosity. An uplift in the value of Hartmann number M diminishes the fluid velocity $\hat{g}'(\eta)$ as a boost in M generates a larger amount of Lorentz force. A coincident impact of β and M is observed on $\hat{g}'(\eta)$.

The ANNs-RBAF-PSO solver demonstrates the potential to provide excellent accuracy in the analysis of challenging fluid dynamics scenarios with complex nonlinear behavior and provides a compelling alternative method for future investigations. Its ability to handle complex fluid problems with high-order nonlinearities opens avenues for investigating a wide range of phenomena and offers researchers a robust tool to deepen their understanding of fluid dynamics and its applications in various fields [71–78].

Data Availability

No data is associated with the manuscript.

CRediT Authorship Contribution Statement

Zeeshan Ikram Butt: Writing – review & editing, Writing – original draft, Methodology, Investigation, Formal analysis, Conceptualization. Iftikhar Ahmad: Validation, Supervision, Software, Resources, Investigation, Data curation. Muhammad Shoaib: Writing – review & editing, Supervision, Software, Resources, Project administration, Methodology. Syed Ibrar Hussain: Writing – review & editing, Writing – original draft, Methodology, Investigation, Funding acquisition, Conceptualization. Hira Ilyas: Writing – review & editing, Validation, Software, Resources, Formal analysis, Conceptualization. Muhammad Asif Zahoor Raja: Writing – review & editing, Visualization, Validation, Supervision, Software, Formal analysis, Conceptualization.

Declaration of Interest

The authors declare that they have no known competing financial interests or personal relationships that could have appeared to influence the work reported in this paper.

Nomenclature

A, C	fluid parameters
B	magnetic field strength
M	Hartmann number
$U(x)$	stretching velocity
u_1, u_2	components of velocity, $m \cdot s^{-1}$
ν_g	kinematic viscosity, $m^2 \cdot s^{-1}$
α, β	material parameters
η	dimensionless variable
μ_g	dynamic viscosity, $kg \cdot m^{-1} \cdot s^{-1}$
ρ_g	fluid density, $kg \cdot m^{-3}$
σ_g	electrical conductivity, $S \cdot m^{-1}$
a	velocity coefficient, s^{-1}

References

[1] M. Mishra, L. Panigrahi, J. Panda, Investigation of induced magnetic field on MHD radiative flow across an exponentially stretching sheet, *Int. J. Amb. Energy* 44 (1) (2023) 1192–1201.

[2] A.K. Abdul Jawwad, M. Jawad, K.S. Nisar, M. Saleem, B. Hasanain, Radiative transport of MHD stagnation point flow of chemically reacting Carreau nanofluid due to radially stretched sheet, *Alex. Eng. J.* 69 (2023) 699–714.

[3] U.S. Mahabaleshwar, K.N. Sneha, A. Wakif, Significance of thermo-diffusion and chemical reaction on MHD Casson fluid flows conveying CNTs over a porous stretching sheet, *Waves Random Complex Medium* 10 (2023) 1–19.

[4] A.M. Alqahtani, M. Bilal, M. Usman, T.R. Alsenani, A. Ali, S.R. Mahmuod, Heat and mass transfer through MHD Darcy Forchheimer Casson hybrid nanofluid flow across an exponential stretching sheet, *ZAMM J. Appl. Math. Mech.* 103 (6) (2023) e202200213.

[5] A. Al-Bossly, F.S. Alduais, S. Ahmad Lone, M.Y. Almusawa, A. Saeed, A stratified MHD flow of Eyring–Powell fluid containing gyrotactic microorganisms through a stretching sheet with mixed convection, *ZAMM J. Appl. Math. Mech.* 103 (9) (2023) e202200492.

[6] M.M. Bhatti, E.E. Michaelides, Oldroyd 6-constant Electro-magneto-hydrodynamic fluid flow through parallel micro-plates with heat transfer using Darcy–Brinkman–Forchheimer model: a parametric investigation, *Math. Eng.* 5 (3) (2023) 1–19.

[7] A. Shahid, H.L. Huang, C.M. Khalique, M.M. Bhatti, Numerical analysis of activation energy on MHD nanofluid flow with exponential temperature-dependent viscosity past a porous plate, *J. Therm. Anal. Calorim.* 143 (3) (2021) 2585–2596.

[8] M. Abbas, M. Bhatti, M. Rashidi, Heat transfer on magnetohydrodynamic stagnation point flow through a porous shrinking/stretching sheet: a numerical study, *Therm. Sci.* 24 (2 Part B) (2020) 1335–1344.

[9] K. Ramesh, D. Tripathi, M.M. Bhatti, K. Ghachem, S.U. Khan, L. Kolsi, Mathematical modeling and simulation of electromagnetohydrodynamic bio-nanomaterial flow through physiological vessels, *J. Appl. Biomater. Funct. Mater.* 20 (2022) 22808000221114708.

[10] M.M. Bhatti, L. Phali, C.M. Khalique, Heat transfer effects on electro-magnetohydrodynamic Carreau fluid flow between two micro-parallel plates with Darcy–Brinkman–Forchheimer medium, *Arch. Appl. Mech.* 91 (4) (2021) 1683–1695.

[11] A. Singh, S.C. Sharma, Behaviour of conical porous hybrid journal bearing operated with MHD lubricant considering influence of surface irregularities, *Tribol. Int.* 174 (2022) 107730.

[12] J.R. Lin, MHD steady and dynamic characteristics of wide tapered-land slider bearings, *Tribol. Int.* 43 (12) (2010) 2378–2383.

[13] N.B. Naduvinamani, B.N. Hanumagowda, S. Tasneem Fathima, Combined effects of MHD and surface roughness on couple-stress squeeze film lubrication between porous circular stepped plates, *Tribol. Int.* 56 (2012) 19–29.

[14] M. Nabhani, M. El Khlifi, Inertial MHD couple stress effects on infinitely wide slider bearings, *Tribol. Trans.* 58 (2) (2015) 374–383.

[15] M. Nabhani, M. El Khlifi, Non-Newtonian inertial magnetohydrodynamic porous squeeze film lubrication between circular discs, *Tribol. Int.* 94 (2016) 373–382.

[16] S.R. Munjam, K. Gangadhar, R. Seshadri, M. Rajeswar, Novel technique MDDIM solutions of MHD flow and radiative Prandtl–Eyring fluid over a stretching sheet with convective heating, *Int. J. Amb. Energy* 43 (1) (2022) 4850–4859.

[17] Z. Ullah, I. Ullah, G. Zaman, T.C. Sun, A numerical approach to interpret melting and activation energy phenomenon on the magnetized transient flow of Prandtl–Eyring fluid with the application of Cattaneo–Christov theory, *Wave Random Complex* 2 (2022) 1–21.

[18] M. Shoaib, I. Naz, M.I. Khan, M.A.Z. Raja, G. Zubair, K.S. Nisar, K. Guedri, Artificial intelligence knacks-based stochastic paradigm to study lie group analysis with the impact of electric field on MHD Prandtl–Eyring fluid flow system, *Int. J. Mod. Phys. B* 36 (30) (2022) 2250216.

[19] I. Ullah, R. Ali, H. Nawab, Abdussatar, I. Uddin, T. Muhammad, I. Khan, K.S. Nisar, Theoretical analysis of activation energy effect on Prandtl–Eyring nanoliquid flow subject to melting condition, *J. Non Equilib. Thermodyn.* 47 (1) (2022) 1–12.

[20] S.O. Salawu, Two-step exothermic reaction–diffusion of hydromagnetic Prandtl–Eyring viscous heating fluid in a channel, *Int. J. Thermofluids* 17 (2023) 100300.

[21] Z. Shah, M. Rooman, M. Shutaywi, Computational analysis of radiative engine oil-based Prandtl–Eyring hybrid nanofluid flow with variable heat transfer using the Cattaneo–Christov heat flux model, *RSC Adv.* 13 (6) (2023) 3552–3560.

[22] A.K. Verma, K. Bhattacharyya, S. Rajput, M.S. Mandal, A.J. Chamkha, D. Yadav, Buoyancy driven non-Newtonian Prandtl-Eyring nanofluid flow in Darcy–Forchheimer porous medium over inclined non-linear expanding sheet with double stratification, *Wave Random Complex* 7 (2022) 1–33.

[23] S. Chaudhary, K.K. Chouhan, Darcy–Forchheimer flow of Prandtl-Eyring nanofluid subjected to a Riga plate of varying thickness along with Brownian diffusion, thermophoresis and non-uniform heat source/sink effects, *Numer. Heat Transf. Part A Appl.* 84 (7) (2023) 732–759.

[24] Z.I. Butt, I. Ahmad, M. Shoaib, H. Ilyas, A.K. Kiani, M.A.Z. Raja, Neuro-evolution heuristics for Prandtl–Eyring nanofluid flow with homogenous/heterogeneous reaction across a linearly heated stretched sheet, *Wave Random Complex* 12 (2023) 1–47.

[25] S.O. Salawu, A.M. Obalalu, M. Shamshuddin, Nonlinear solar thermal radiation efficiency and energy optimization for magnetized hybrid Prandtl–Eyring nanoliquid in aircraft, *Arab. J. Sci. Eng.* 48 (3) (2023) 3061–3072.

[26] J. Akram, N.S. Akbar, E. Maraj, Chemical reaction and heat source/sink effect on magnetonano Prandtl–Eyring fluid peristaltic propulsion in an inclined symmetric channel, *Chin. J. Phys.* 65 (2020) 300–313.

[27] M.A.Z. Raja, A. Mehmood, S. Ashraf, K.M. Awan, P. Shi, Design of evolutionary finite difference solver for numerical treatment of computer virus propagation with countermeasures model, *Math. Comput. Simul.* 193 (2022) 409–430.

[28] N. Anwar, I. Ahmad, A.K. Kiani, S. Naz, M. Shoaib, M.A.Z. Raja, Intelligent predictive stochastic computing for nonlinear differential delay computer virus model, *Wave Random Complex* 12 (2022) 1–29.

[29] N. Anwar, I. Ahmad, M.A.Z. Raja, S. Naz, M. Shoaib, A.K. Kiani, Artificial intelligence knacks-based stochastic paradigm to study the dynamics of plant virus propagation model with impact of seasonality and delays, *Eur. Phys. J. Plus* 137 (1) (2022) 144.

[30] S. Noinang, M. Munawar, M.A. Zahoor Raja, Z. Sabir, T. Botmart, W. Weera, P. Junsawang, Numerical assessments employing neural networks for a novel drafted anti-virus subcategory in a nonlinear fractional-order SIR differential system, *IEEE Access* 10 (2022) 114192–114202.

[31] E.B. Moustafa, A. Elsheikh, Predicting characteristics of dissimilar laser welded polymeric joints using a multi-layer perceptrons model coupled with Archimedes optimizer, *Polymers* 15 (1) (2023) 233.

[32] S. Saurav, R. Saini, S. Singh, A dual-channel ensembled deep convolutional neural network for facial expression recognition in the wild, *Comput. Intell.* 39 (5) (2023) 666–706.

[33] M. Shoaib, R. Tabassum, M.A.Z. Raja, K.S. Nisar, M.S. Alqahtani, M. Abbas, A design of predictive computational network for transmission model of Lassa fever in Nigeria, *Results Phys.* 39 (2022) 105713.

[34] A.H. Elsheikh, S.W. Sharshir, M. Abd Elaziz, A.E. Kabeel, G.L. Wang, H.O. Zhang, Modeling of solar energy systems using artificial neural network: a comprehensive review, *Sol. Energy* 180 (2019) 622–639.

[35] A.H. Elsheikh, V.P. Katekar, O.L. Muskens, S.S. Deshmukh, M.A. Elaziz, S.M. Dabour, Utilization of LSTM neural network for water production forecasting of a stepped solar still with a corrugated absorber plate, *Process. Saf. Environ. Prot.* 148 (2021) 273–282.

[36] A. Bamasag, F.A. Essa, Z.M. Omara, E. Bahgat, A.O. Alsaiari, H. Abulkhair, R.A. Alsulami, A.H. Elsheikh, Machine learning-based prediction and augmentation of dish solar distiller performance using an innovative convex stepped absorber and phase change material with nanoadditives, *Process. Saf. Environ. Prot.* 162 (2022) 112–123.

[37] A. Rizwan, I. Ahmad, M.A.Z. Raja, M. Shoaib, Design of spline–evolutionary computing paradigm for nonlinear thin film flow model, *Arab. J. Sci. Eng.* 46 (9) (2021) 9279–9299.

[38] I. Ahmad, M.A.Z. Raja, H. Ramos, M. Bilal, M. Shoaib, Integrated neuro-evolution-based computing solver for dynamics of nonlinear corneal shape model numerically, *Neural Comput. Appl.* 33 (11) (2021) 5753–5769.

[39] A.H. Elsheikh, Applications of machine learning in friction stir welding: prediction of joint properties, real-time control and tool failure diagnosis, *Eng. Appl. Artif. Intell.* 121 (2023) 105961.

[40] M. Shoaib, M. Kausar, K.S. Nisar, M. Asif Zahoor Raja, A. Morsy, Impact of thermal energy on MHD Casson fluid through a Forchheimer porous medium with inclined non-linear surface: a soft computing approach, *Alex. Eng. J.* 61 (12) (2022) 12211–12228.

[41] S.I. Hussain, I. Ahmad, N. Yasmeen, The remarkable role of hydrogen in conductors with copper and silver nanoparticles by mixed convection using viscosity Reynold's model, in: Proceedings of the International Conference on Nonlinear Dynamics and Applications, China, 2024, pp. 49–60.

[42] M. Abd Elaziz, F.A. Essa, A.H. Elsheikh, Utilization of ensemble random vector functional link network for freshwater prediction of active solar stills with nanoparticles, *Sustain. Energy Technol. Assess.* 47 (2021) 101405.

[43] Z.I. Butt, I. Ahmad, M.A.Z. Raja, S.I. Hussain, M. Shoaib, H. Ilyas, Neuro-heuristic computational intelligence approach for optimization of electro-magneto-hydrodynamic influence on a nano viscous fluid flow, *Int. J. Intell. Syst.* 2023 (2023) 7626478.

[44] Z.I. Butt, I. Ahmad, S.I. Hussain, M.A.Z. Raja, M. Shoaib, H. Ilyas, Inverse multiquadric kernel-based neuro heuristic approach to analyze the unsteady MHD nanofluid flow *via* permeable elongating surface, *ZAMM J. Appl. Math. Mech.* 104 (2) (2024) e202300390.

[45] Z.I. Butt, I. Ahmad, S.I. Hussain, M.A.Z. Raja, M. Shoaib, H. Ilyas, Intelligent computing paradigm for unsteady magneto nano-polymeric Casson nanofluid with Ohmic dissipation and thermal radiation, *Chin. J. Phys.* 88 (2024) 212–269.

[46] I. Ahmad, S.I. Hussain, H. Ilyas, L. Zoubir, M. Javed, M.A. Zahoor Raja, Integrated stochastic investigation of singularly perturbed delay differential equations for the neuronal variability model, *Int. J. Intell. Syst.* 2023 (2023) 1918409.

[47] I. Ahmad, H. Ilyas, S.I. Hussain, M.A.Z. Raja, Evolutionary techniques for the solution of bio-heat equation arising in human dermal region model, *Arab. J. Sci. Eng.* 49 (3) (2024) 3109–3134.

[48] I. Ahmad, S.I. Hussain, H. Ilyas, M.A.Z. Raja, S. Afzal, M. Javed, Optimal control of thermoregulation in the human dermal regions investigated through the stochastic integrated techniques, *Case Stud. Therm. Eng.* 58 (2024) 104381.

[49] S.I. Hussain, I. Ahmad, M.A.Z. Raja, C.M.Z. Umer, A computational convection analysis of SiO_2/water and MoS_2-SiO_2/water based fluidic system in inverted cone, *Eng. Rep.* 5 (11) (2023) e12660.
[50] I. Ahmad, S.I. Hussain, M.A.Z. Raja, M. Shoaib Qurratulain, Transportation of hybrid MoS_2–SiO_2/EG nanofluidic system toward radially stretched surface, *Arab. J. Sci. Eng.* 48 (1) (2023) 953–966.
[51] S.I. Hussain, E. Toscano, An extensive investigation into the use of machine learning tools and deep neural networks for the recognition of skin cancer: challenges, future directions, and a comprehensive review, *Symmetry* 16 (3) (2024) 366.
[52] I. Ahmad, H. Qureshi, M.A. Zahoor Raja, S.I. Hussain, S. Fatima, A novel design of stochastic approximation treatment of longitudinal rectangular fin dynamical model, *Case Stud. Therm. Eng.* 54 (2024) 104042.
[53] D.A. Tiwari, RMCL: a deep learning based recursive malicious context learner in social networks, *Comput. Intell.* 38 (6) (2022) 1956–1989.
[54] Z. Kowalczuk, M. Czubenko, W. Żmuda-Trzebiatowska, Categorization of emotions in dog behavior based on the deep neural network, *Comput. Intell.* 38 (6) (2022) 2116–2133.
[55] R.J. Rajappan, T. Kondampatti Kandaswamy, A composite framework of deep multiple view human joints feature extraction and selection strategy with hybrid adaptive sunflower optimization-whale optimization algorithm for human action recognition in video sequences, *Comput. Intell.* 38 (2) (2022) 366–396.
[56] F. Rustam, I. Ashraf, R. Shafique, A. Mehmood, S. Ullah, G. Sang Choi, Review prognosis system to predict employees job satisfaction using deep neural network, *Comput. Intell.* 37 (2) (2021) 924–950.
[57] S. Ayub, N. Singh, M.Z. Hussain, M. Ashraf, D.K. Singh, A. Haldorai, Hybrid approach to implement multi-robotic navigation system using neural network, fuzzy logic, and bio-inspired optimization methodologies, *Comput. Intell.* 39 (4) (2023) 592–606.
[58] A. Hussain, M.Y. Malik, M. Awais, T. Salahuddin, S. Bilal, Computational and physical aspects of MHD Prandtl–Eyring fluid flow analysis over a stretching sheet, *Neural Comput. Appl.* 31 (1) (2019) 425–433.
[59] R. Eberhart, J. Kennedy, Particle swarm optimization, in: Proceedings of the IEEE International Conference on Neural Networks, Perth, Australia, 1995, pp. 1942–1948.
[60] I. Ahmad, S.U.I. Ahmad, K. Kutlu, H. Ilyas, S.I. Hussain, F. Rasool, On the dynamical behavior of nonlinear Fitzhugh–Nagumo and Bateman–Burger equations in quantum model using Sinc collocation scheme, *Eur. Phys. J. Plus* 136 (11) (2021) 1108.
[61] D.P. Rangasamy, S. Rajappan, A. Natarajan, R. Ramasamy, D. Vijayakumar, Variable population-sized particle swarm optimization for highly imbalanced dataset classification, *Comput. Intell.* 37 (2) (2021) 873–890.
[62] T. Botmart, Z. Sabir, M. Asif Zahoor Raja, W. Weera, M.R. Ali, R. Sadat, A.A. Aly, Alosaimy, A. Saad, A hybrid swarming computing approach to solve the biological nonlinear Leptospirosis system, *Biomed. Signal Process. Contr.* 77 (2022) 103789.
[63] I. Ahmad, S.I. Hussain, H. Ilyas, J.L. García Guirao, A. Ahmed, S. Rehmat, T. Saeed, Numerical solutions of Schrödinger wave equation and transport equation through Sinc collocation method, *Nonlinear Dyn.* 105 (1) (2021) 691–705.
[64] F. Altaf, C.L. Chang, N.I. Chaudhary, K.M. Cheema, M.A.Z. Raja, C.M. Shu, A.H. Milyani, Novel fractional swarming with key term separation for input nonlinear control autoregressive systems, *Fractal Fract.* 6 (7) (2022) 348.
[65] N.A. Malik, C.L. Chang, N.I. Chaudhary, M.A.Z. Raja, K.M. Cheema, C.M. Shu, S. S. Alshamrani, Knacks of fractional order swarming intelligence for parameter estimation of harmonics in electrical systems, *Mathematics* 10 (9) (2022) 1570.
[66] J. Nocedal, S.J. Wright, Numerical Optimization, Springer, New York, 1999.
[67] M. Shoaib, S. Kainat, M.A.Z. Raja, K.S. Nisar, Design of artificial neural networks optimized through genetic algorithms and sequential quadratic programming for tuberculosis model, *Wave Random Complex* 6 (2022) 1–24.
[68] Z.I. Butt, I. Ahmad, H. Ilyas, M. Shoaib, M.A.Z. Raja, Design of inverse multiquadric radial basis neural networks for the dynamical analysis of MHD casson nanofluid flow along a nonlinear stretchable porous surface with multiple slip conditions, *Int. J. Hydrog. Energy* 48 (42) (2023) 16100–16131.
[69] Z.I. Butt, I. Ahmad, M. Shoaib, H. Ilyas, M.A.Z. Raja, A novel design of inverse multiquadric radial basis neural networks to analyze MHD nanofluid boundary layer flow past a wedge embedded in a porous medium under the influence of radiation and viscous effects, *Int. Commun. Heat Mass Transf.* 140 (2023) 106516.
[70] Z.I. Butt, I. Ahmad, M. Shoaib, H. Ilyas, M.A.Z. Raja, Electro-magnetohydrodynamic impact on Darrcy–Forchheimer viscous fluid flow over a stretchable surface: integrated intelligent neuro-evolutionary computing approach, *Int. Commun. Heat Mass Transf.* 137 (2022) 106262.
[71] W. da Silva Cotrim, J.C. Coimbra, K.C.F. Cotrim, Modeling and simulation of broiler carcass precooling by computational fluid dynamics, *J. Food Process. Eng.* 44 (6) (2021) e13693.
[72] R. de Oliveira Vieira, J.L. Silva Jr., P.A. Meira, G.L. Bressan, P.V.C. Calvo, H.S. Santana, M.S. Palma, Experimental and numerical investigation of the reaction of 2,4-thiazolidinedione and *p*-methoxybenzaldehyde in microreactors for the production of drugs for diabetes mellitus type 2 treatment, *Can. J. Chem. Eng.* 101 (11) (2023) 6505–6520.
[73] I. Ahmad, S.I. Hussain, M. Usman, H. Ilyas, On the solution of Zabolotskaya–Khokhlov and diffusion of oxygen equations using a Sinc collocation method, *Partial. Differ. Equ. Appl. Math.* 4 (2021) 100066.
[74] M. Rezaeimanesh, S. Ali Asghar Ghoreyshi, S.M. Peyghambarzadeh, S.H. Hashemabadi, Coke deposition and run length in industrial naphtha thermal cracking furnaces *via* a quasi-steady state coupled CFD model, *Can. J. Chem. Eng.* 101 (7) (2023) 3856–3873.
[75] L.J. Zhang, M.M. Bhatti, O.A. Bég, H.J. Leonard, S. Kuharat, Numerical study of natural convection dissipative electro-magnetic non-Newtonian flow through a non-Darcy channel, *ZAMM J. Appl. Math. Mech.* 102 (10) (2022) e202100608.
[76] M.M. Bhatti, S.M. Sait, R. Ellahi, Magnetic nanoparticles for drug delivery through tapered stenosed artery with blood based non-Newtonian fluid, *Pharmaceuticals* 15 (11) (2022) 1352.
[77] I. Ahmad, S. Ibrar Hussain, H. Ilyas, S. Jabeen, A. Iqrar, On the applications of collocation method for numerically analyzing the nonlinear Degasperis–Procesi and Benjamin–Bona–Mahony equations, *Int. J. Mod. Phys. B* 38 (20) (2024) 2450264.
[78] E.F. Toro, M. Celant, Q. Zhang, C. Contarino, N. Agarwal, A. Linninger, L.O. Müller, Cerebrospinal fluid dynamics coupled to the global circulation in holistic setting: mathematical models, numerical methods and applications, *Int. J. Numer. Method. Biomed. Eng.* 38 (1) (2022) e3532.